STOCHASTIC UNDERSEEPAGE ANALYSIS IN DAMS

by

(GARY) E. B. CHOOT

B.Sc. University of Alberta
(1978)

SUBMITTED IN PARTIAL FULFILLMENT
OF THE REQUIREMENTS FOR THE
DEGREE OF

MASTER OF SCIENCE

at the

MASSACHUSETTS INSTITUTE OF TECHNOLOGY

May 1980

Signature of Author Gary L. B. Choot

Department of Civil Engineering
May 19,1980

Certified by Erik H. Vanmarcke

Thesis Supervisor

Accepted by

Chairman, Department Committee

STOCHASTIC UNDERSEEPAGE ANALYSIS IN DAMS

by

GARY E. B. CHOOT

Submitted to the Department of Civil Engineering
on May 19, 1980 in partial fulfillment of the
requirements for the Degree of Master of Science in
Civil Engineering

ABSTRACT

A first-order second-moment approach is used to quantify the uncertainty of piezometric heads due to the inherent spatial varaibility of permeability in the field. Permeability is modelled as a spatial random process characterized by its mean, its standard deviation, and its scale of fluctuation.

The results of the first-order second-moment analysis are applied to the study of seepage-related problems in the foundations of dams. Examples are given to show the use of the method to interpret readings of piezometers installed to monitor the performance of active seepage control features in dam foundations.

Thesis Supervisor: Dr. Erik H. Vanmarcke

Title: Professor of Civil Engineering

ACKNOWLEDGEMENTS

I am indebted to professor Vanmarcke for his help and supervision of this work. I also wish to express my gratitude to Professor Whitman for his valuable suggestions and guidance during the course of this work.

My parents, brothers and sister deserve special appreciation for the encouragement and moral support they provide especially during these past two years.

I also like to thank Lisa Magnano for doing an excellent job of typing this thesis.

This work was supported by the National Science Foundation Grant PFR-7815898.

TABLE OF CONTENTS

PAGE

LIST OF FIGURES

LIST OF TABLES

CHAPTER I INTRODUCTION

The underseepage behavior of a dam may be studied in many ways. One of the most effective means is an observational approach based on piezometer measurements. Meaningful interpretation of piezometer readings, however, cannot be achieved unless one understands the sources of uncertainty of the readings.

In this study, we attribute the discrepancy between measured and predicted piezometer readings to three causes. They are:

(i) inherent variability

(ii) instrument error

(iii) modelling error

Inherent variability of piezometric head exists because of the intrinsic uncertainty of permeability governing the seepage of water through any soil mass. It is the background uncertainty that is always present in an engineer's prediction. In theory, the inherent variability can be eliminated if an engineer can determine the exact permeability at every point within the soil mass and take the details of this permeability field into consideration in his analysis. Instead of trying to eliminate the inherent variability, an easier and more practical way is to account for this variability directly in his prediction, which is only feasible through probabilistic treatment of seepage.

The causes of instrument error can be direct or indirect. Malfunctioning and improper calibration of piezometers are two examples of the direct causes of instrument errors. Sampling and testing errors associated with laboratory and field tests that provide permeability values used in

seepage analysis can be regarded as the indirect causes of instrument error. Instrument error can be minimized by proper calibration of equipments used. However, the calibration of equipments can be inaccurate if the magnitude of the inherent variability is unknown.

In general, the modelling error can be attributed to (i) inaccurate method of analysis, and (ii) incomplete information about the soil mass. The first cause is not much of a problem in underseepage analysis because D'arcy's law that describes seepage through porous media appears to be valid for seepage situations of interest to a geotechnical engineer. Because of the incomplete information about the soil mass, an engineer has to make certain assumptions about the soil properties to arrive at his final design. He has to depend on instrumentation to check the modelling error. For example, he can check the validity of his assumptions about the permeability distribution by comparing predicted and observed piezometer readings. Of course, any logical deduction cannot be made without properly accounting for the inherent variability and the instrument error.

The main objectives of this thesis are:

(i) to develop a procedure for quantifying the uncertainty of piezometric heads due to the inherent variability of permeability,

(ii) to apply the knowledge about the uncertainty of piezometric heads to the study of active seepage control measures in the foundation of a dam.

We use a first-order second-moment (FOSM) approach to quantify the uncertainty of piezometric heads due to the inherent spatial variability of permeability. Permeability is modelled as a spatial random process

characterized by its mean, its standard deviation, and its scale of fluctuation (Vanmarcke 1979a).

In Chapter II, we describe the basic methodology for quantifying the inherent variability of piezometric heads. Parametric studies on a 1-D and a 2-D models are carried out in Chapters III and IV respectively. The results from Chapters III and IV are then applied to the study of active seepage control measures in the foundation of a dam in Chapter V. Some other potential applications of the methodology are also discussed. Throughout the thesis, measurement errors are neglected.

CHAPTER II BASIC METHODOLOGY

2.1 First Order Second Moment (FOSM) Approach

Information about variability in head can be predicted from input variability in permeability by using the first-order second-moment (FOSM) approach. The following sections will discuss the four steps which are necessary in order to adopt the FOSM approach for the underseepage problem being studied:

1. Discretization of the underseepage path into n equal size elements with m nodal points.

Statistical homogeneity is assumed for the medium. Each of the elements has a permeability k_i which represents the spatial average of permeability over the element. It is convenient but not necessary to choose equal size elements. By doing so, statistical homogeneity is maintained for the spatial averages.

One immediate concern about this type of discretization is the extent to which the result is affected by the process of discretization of a continuum. Bear (1972) suggested the use of representative elementary volume (REV). Conceptually, a medium discretized into volumes equal to or smaller than REV can, for all practical purposes, be treated as continuous. The obvious difficulty of the approach is in the determination of REV, which is no more than just a hypothetical quantity. It is better to follow an approach which is not too sensitive to discretization. In Chapter III, the relevance of REV to the underseepage study will be examined further.

2. Linearization of the functional relationship between nodal head (h_j) and element permeability (k_i).

The FOSM approach is only exact if all the h_js can be expressed as a linear combination of all the k_is. For a nonlinear function, the FOSM approach becomes an approximation whose accuracy decreases with increasing nonlinearity of the function.

Linearization in the FOSM approach can be expressed in the following form:

$$\text{if } \underline{h} = f(\underline{k}) \qquad \text{where } \begin{matrix} \underline{h} \text{ is } m \times 1 \\ \underline{k} \text{ is } n \times 1 \end{matrix} \tag{2.1}$$

where $\underline{h}$ is a matrix. Using Taylor's expansion, we have:

$$\underline{h} = \underline{h}_o + f'(\underline{k}_o)(\underline{k} - \underline{k}_o) + \frac{1}{2} f''(\underline{k}_o)(\underline{k} - \underline{k}_o)^2 + \cdots \text{ higher order terms} \tag{2.2}$$

The reason that the FOSM approach is only an approximation is that second and higher order terms in the above Taylor's expansion are discarded. Thus, equation 2.1 can be written in its linearized form:

$$\underline{h} = \underline{h}_o + \underline{A}(\underline{k} - \underline{k}_o) \qquad \begin{matrix} \underline{A} = f'(\underline{k}_o) \\ \underline{h}_o = f(\underline{k}_o) \end{matrix} \tag{2.3}$$

$\underline{A}$ is defined as the sensitivity matrix. Its element A_{ji} is by definition the partial derivative of h_j with respect to k_i (i.e., $\partial h_j/\partial k_i$) evaluated at the means of all the k_is. $\partial h_j/\partial k_i$ can be approximated as $\Delta h_j/\Delta k_i$ in which Δk_i can be any chosen permeability increment away from the mean. A reasonable choice of Δk_i would be one standard deviation of k; so that $\Delta h_j/\Delta k_i$ becomes the average effect, over one standard deviation, of an increase or decrease of k_i on h_j.

The sensitivity matrix, $\underline{A}$, for the underseepage problem is calculated with the aid of a modified version of the FEDAR (Finite Element analysis of DARcy flow problems) computer program. The original version of FEDAR was developed by Taylor and Brown (1967). This modified program first calculates $\underline{h}_o$, which contains the nodal potentials for the case when all the element permeabilities are constant and equal to the mean permeability (m_k). It then iterates to find $\underline{h}_1$, which contains the nodal potentials for the case when all the element permeabilities are equal to m_k except k_1, which is equal to $m_k + \Delta k_1$. The column matrix $(\underline{h}_1 - \underline{h}_o)/\Delta k_1$ is the same as the first column of $\underline{A}$. $\underline{h}_2$ is obtained in a similar fashion, by changing k_2 to $m_k + \Delta k_2$ but keeping other permeabilities at m_k. Again, $(\underline{h}_2 - \underline{h}_o)/\Delta k_2$ is taken as the second column of $\underline{A}$. The above procedure is repeated for all other columns of $\underline{A}$.

3. Derivation of the covariance matrix for spatial averages of permeability.

In FOSM analysis, the necessary statistical information about permeability is assumed to be fully described by its mean, its standard deviation, and its spatial correlation structure. Only the standard deviation and spatial correlation structure are needed in this section for the derivation of the covariance matrix for permeability.

Variance of the permeability can be obtained from straightforward statistical analysis of permeability data by taking advantage of the assumed stationary property of permeability. The distribution of permeability can be assumed to be lognormal (Freeze 1975). Freeze also presented a collection of statistical information about variability in permeability by different investigators.

Spatial correlation structure for permeability is harder to determine. Because the underlying geological process behind every formation and deposit is highly complicated, it is doubtful if the spatial correlation structure for soil permeability will ever be determined exactly. Bakr et al (1978) indicated that negative exponential correlation function can adequately represent some of Bakr's (1976) field data on permeability. However, they realized that the exponential function cannot be used for 1-D seepage analysis because of the existence of singularity. They had to use a different correlation function for 1-D analysis. Smith and Freeze (1979) used the "nearest neighbor" correlation for their Monte Carlo simulation. None of the above approach guarantees realistic representation of permeability behavior.

This study adopts an alternative approach. The approach follows directly from Vanmarcke's (1979a) research on spatial averages and the scale of fluctuation of random functions. According to Vanmarcke, much of the information about spatial random function is contained in its mean, its variance and its scale of fluctuation. Scale of fluctuation, θ, can be defined in several ways. One way is to define θ as the area underneath the correlation function from minus infinity to plus infinity:

$$\theta = \int_{-\infty}^{+\infty} \rho(\tau)\, d\tau$$

$\rho(\tau)$ = correlation function

τ = separation distance.

θ represents the distance over which significant amount correlation between the variances at two points in space can be expected. It is exactly twice the macroscale defined by Dagan (1979). Parameters of many theoretical correlation functions can be expressed in terms of θ. For example, for two

different exponential correlation functions, we have:

$$\rho(\tau) = e^{-(a\tau)^2} \qquad a = \sqrt{\pi}/\theta$$
$$\rho(\tau) = e^{-a\tau} \qquad a = 2/\theta \tag{2.4}$$

It was pointed out earlier that none of the existing theoretical correlation functions is believed to be able to describe the spatial behavior of permeability for all cases. For the underseepage study in this paper, a simple triangular correlation function shown in Fig. 2.1 will be employed for 1-D analysis.

The form of the triangular correlation function is:

$$\rho(\tau) = \begin{cases} 1 - |\tau|/\theta & |\tau| \leq \theta \\ 0 & \text{elsewhere} \end{cases} \tag{2.5}$$

and the corresponding variance reduction function is:

$$\Gamma^2(T) = \begin{cases} 1 - (T/3\theta) & T \leq \theta \\ (\theta/T)[1 - (\theta/3T)] & T \geq \theta \end{cases} \tag{2.6}$$

Depending on the averaging interval T, the variance reduction function can have a value anywhere between 0 and 1. Point variance of permeability has to be multiplied by this variance reduction function to obtain the variance of the spatial average of an interval of length T.

Besides being simple and analytical tractable, the triangular correlation function also has the desirable property of yielding a variance reduction function, Eq. 2.6, which is somewhat an "average" of the variance

reduction functions calculated from other correlation functions. Fig. 2 from Vanmarcke (1979a) has been reproduced in Fig. 2.2. here to show the effect.

For 1-D spatial functions, Vanmarcke (1979a) derived the covariance for spatial averages as being:

$$\mathrm{Cov}[y_{T_1}, y_{T_2}] = \frac{\sigma_k^2}{2T_1T_2}\left\{T_o^{*2}\,\Gamma^2(T_o^*) - T_1^{*2}\,\Gamma^2(T_1^*) - T_3^{*2}\,\Gamma^2(T_3^*) + T_2^{*2}\,\Gamma^2(T_2^*)\right\} \tag{2.7a}$$

More concisely, Eq. 2.7a becomes

$$\mathrm{Cov}[y_{T_1}, y_{T_2}] = \frac{\sigma_k^2}{2T_1T_2}\sum_{i=0}^{3}(-1)^i\,T_i^{*2}\,\Gamma^2(T_i^*) \tag{2.7b}$$

σ_k^2 is the point variance of permeability. y_{T_1} is the spatial average of permeability over an interval T_1. Fig. 2.3 illustrates the meaning of the symbols used in Eqs. 2.7a and b.

Finally, with the basic geometry from the discretization step and a known θ, it is relatively simple to assemble the covariance matrix for spatial averages of permeability.

A 2-D extension of the 1-D formulation given above will be treated in detail in Chapter IV.

4. Formulation of the covariance matrix for hydraulic head.

Information available at this stage are: $\underline{A}$, the sensitivity matrix; $\Sigma_{\underline{k}}$, the covariance matrix of permeability; and σ_y^2, the variance of spatial average. From the linearized relationship between $\underline{h}$ and $\underline{k}$ expressed in Eq. 2.3, FOSM approach permits $\Sigma_{\underline{h}}$, covariance matrix for hydraulic head to be expressed as:

$$\Sigma_{\underline{h}} = \underline{A}\ \Sigma_{\underline{k}}\ \underline{A}^T \tag{2.8}$$

For equal size elements, $\Sigma_{\underline{h}}$ can further be expressed as:

$$\Sigma_{\underline{h}} = \sigma_y^2\ \underline{A}\ C_{\underline{k}}\ \underline{A}^T \tag{2.9}$$

$C_{\underline{k}}$ is the correlation matrix.

2.2 Comment on the Basic Methodology

At present, there are three statistical approaches adoptable to the study of flow through a statistically homogeneous media. They are:

(i) Rigorous solution of the differential equation governing the flow

(ii) Monte Carlo simulation

(iii) FOSM approach.

Detailed discussion of the first approach is not intended here. For more information, see Sagar (1978), Bakr et al (1978) and Dagan (1979). Rigorous solution is very restrictive in its application because it involves too many assumptions. For example, Bakr et al (1978) approach using small perturbation requires that: (a) boundaries for the aquifer are sufficiently far from the region of interest so that a constant head uncertainty is achieved, (b) rigorous correlation structure and exact probability distribution have to be assumed for the permeability and (c) the perturbation is small. None of the above mentioned assumptions is realistic for dams. Another example is Dagan (1979), who derived his results by assuming, besides infinitely far boundaries, that permeability space can be broken up into spherical independent blocks.

The second approach was first used by Warren and Price (1961) and later by Freeze (1975) and Smith and Freeze (1979). Some of the obvious drawbacks of simulation approach are (i) it does not provide a general theory for seepage behavior, i.e., each new problem has to be resolved, (ii) it is inefficient and computationally expensive, (iii) it is hard to introduce a realistic spatial correlation for the block structure used, (iv) discontinuities between adjacent blocks are hard to take care of, and (v) no simple method is available to extend Monte Carlo simulation to 2-D or 3-D studies.

The approach followed by this report is that of the FOSM. Mosely (1979) used a somewhat similar methodology and studied the problem in much lesser detail. Dettinger (1979) also applied the FOSM methodology to study seepage in aquifers. His formulation began with transient flow equation. This makes his approach more suitable for the study of transient behavior of aquifer.

FOSM has some disadvantages, the most important one being that it is only applicable to the class of functions which are not too nonlinear. The restriction arises because of the assumption made in arriving at Eqs. 2.8 and 2.9. For one-dimensional analysis, it will be proved in Chapter III that under certain conditions, the behavior is linear. The behavior of 2-D underseepage model is much more nonlinear than the 1-D case. Chapter III will describe a proposed procedure to compensate for the nonlinearity using the equivalent slope method.

Another restriction of FOSM approach is that only the mean and the variance of the hydraulic head is obtained. It is impossible to extract from the approach information about higher moments which are important if

the exact distribution of hydraulic head is desired.

FOSM approach opens up important aspects of seepage behavior. First of all, it isolates the three major influences on the variability of hydraulic head. Eq. 2.9 shows that head uncertainty is directly related to σ_y^2, variance of the permeability; A, sensitivity of hydraulic head to change in permeability; and C, the extent to which permeability is correlated. Parametric study on any seepage model can be carried out relatively easily. Other advantages of the FOSM approach will be discussed in the course of subsequent chapters.

What is unique about the current approach is the way correlation is being handled. The general philosophy in this study is that is makes more sense to deal with the scale of fluctuation than with the full correlation function of permeability in such a field-oriented problem. Scale of fluctuation of permeability can be estimated by analyzing equally spaced samples using the methodology suggested by Vanmarcke (1979a). The use of triangular function to approximate correlation function is a convenient choice because triangular function has the desirable features of being simple and having a variance function whose shape is the average of other variance functions. Choice of correlation functions is not important as long as their θs match. In any case, if a suitable correlation function is found for permeabilities, the results presented will only be subjected to secondary refinements.

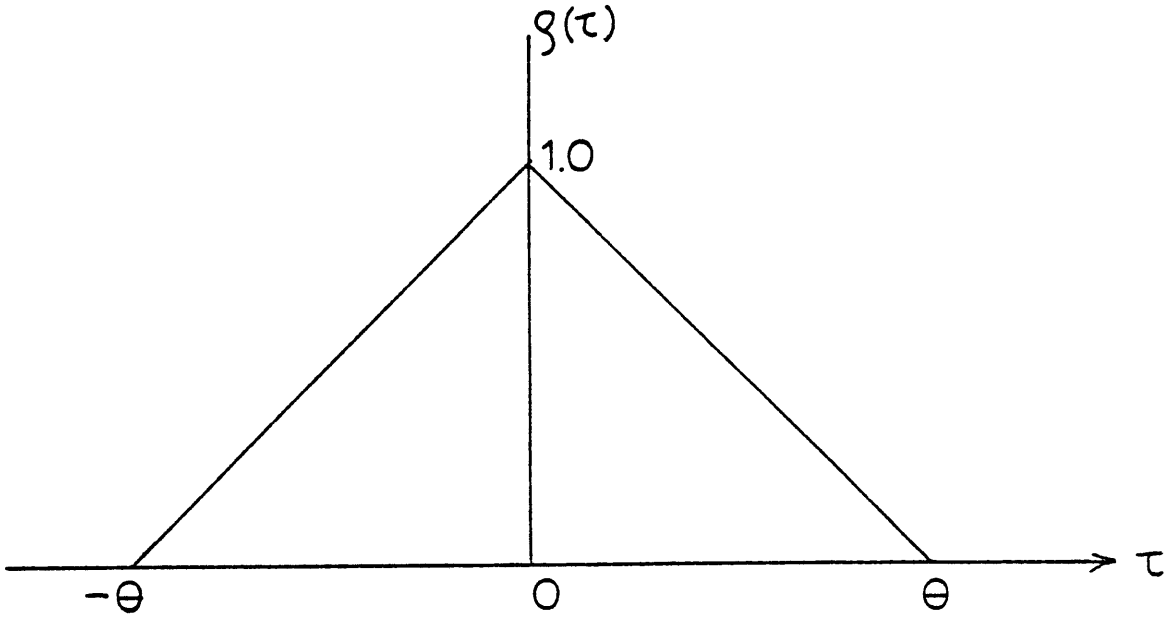

FIG. 2.1 TRIANGULAR CORRELATION FUNCTION

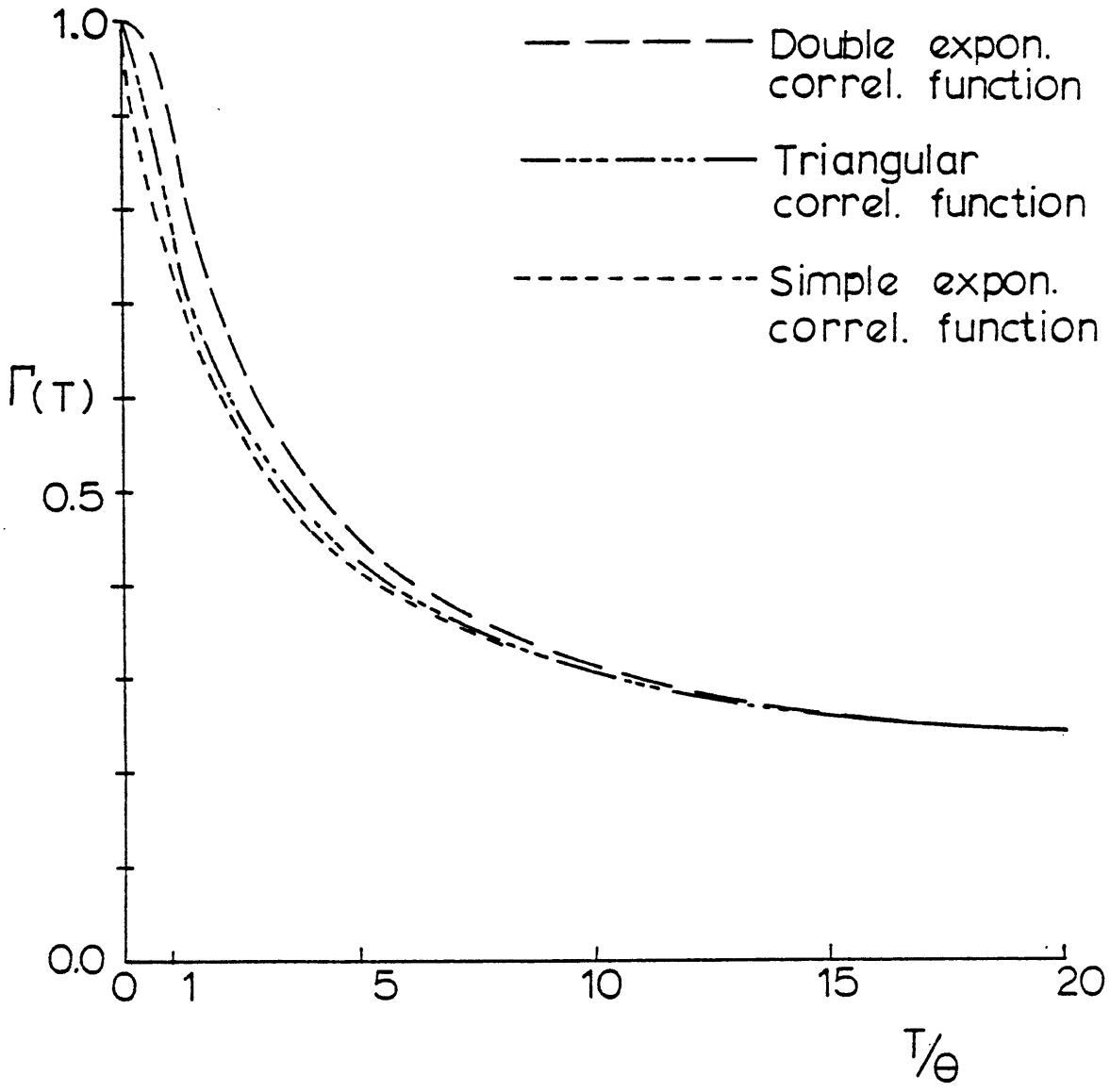

FIG. 2.2 STANDARD DEVIATION REDUCTION FACTOR $\Gamma(T)$

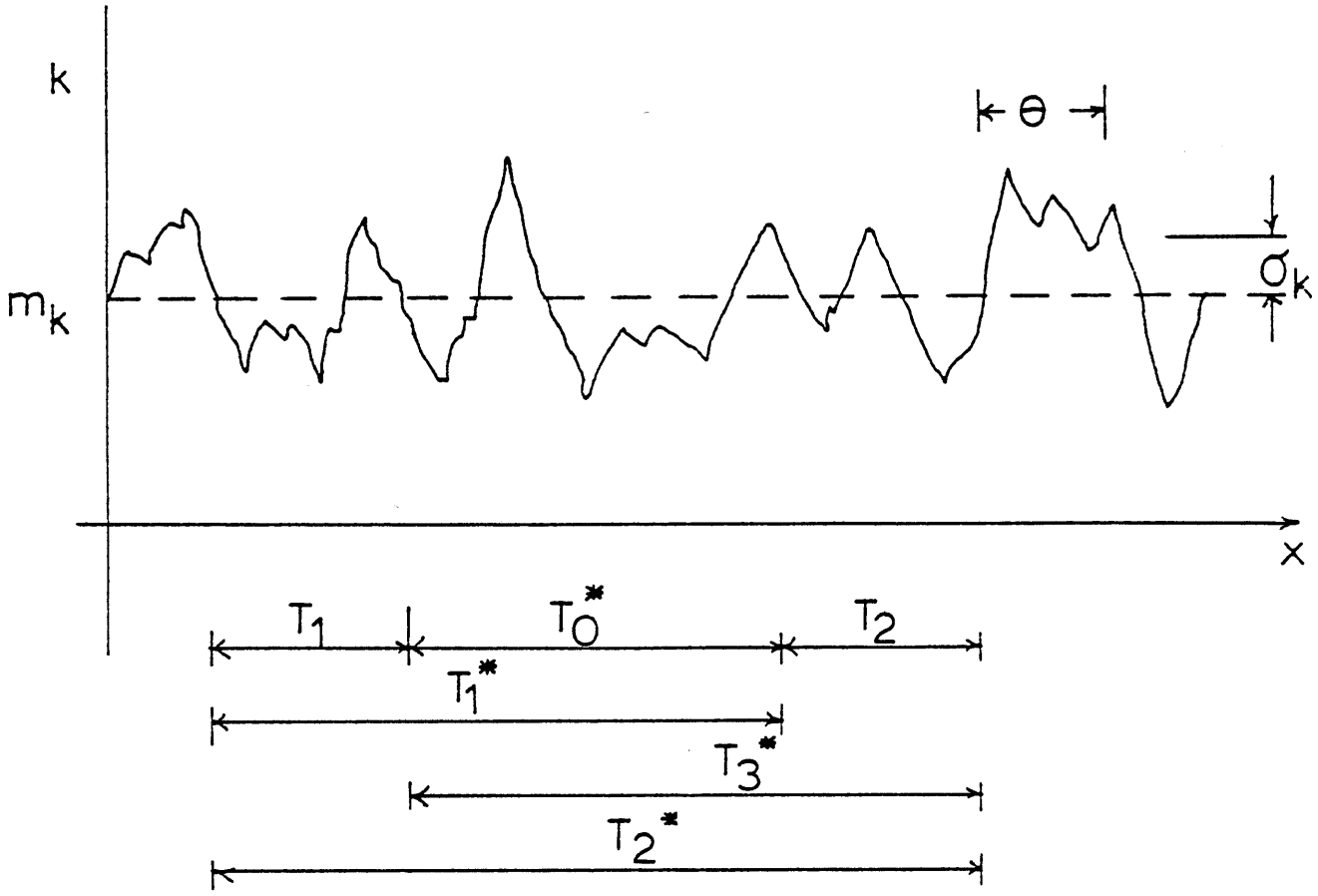

FIG. 2.3 NOTATIONS FOR EQN. 2.6 AND 2.7

CHAPTER III ONE-DIMENSIONAL UNDERSEEPAGE STUDY

In this chapter, the FOSM approach explained in Chapter II will be applied to a one-dimensional underseepage situation.

3.1 Basic One-Dimensional Underseepage Model

(a) Geometry of the basic model

Fig. 3.1 shows the cross section of a typical dam whose underseepage path is 500' long and 100' wide. In order to make the flow truly one-dimensional, the soil upstream as well as downstream of the dam is assumed to be infinitely pervious. Upstream and downstream water elevation are at 100' and 0' respectively. The underseepage path is discretized into 10 equal size elements in series so that the basic model is equivalent to that of Freeze (1975). Hence, it is easy to compare results from the present FOSM analysis with Freeze's results and also with other published results on 1-D seepage analysis, such as Dettinger (1979) and Moseley (1979), which are also based on Freeze's model.

(b) Statistical parameters of the basic model

Permeability is assumed to be lognormally distributed. The basis of the assumption was well explained in Freeze (1975) and will not be elaborated on here. For the basic model, the mean and the standard deviation of log k are chosen to be -1.0 and 0.25 respectively. The mean of -1.0 corresponds to a coefficient of permeability of 0.1 ft/sec which is a realistic value for sand and gravel foundation. It should be emphasized here that 0.25 is the point variance of log k, not the variance of the spatial average of permeability over an element. Scale of fluctuation for this basic model is chosen to be 225 feet.

(c) Correlation matrix of the permeability of the basic model

Based on a simple triangular correlation function together with the known scale of fluctuation, the covariance matrix of the basic model is formulated according to Eq. 2.7. The correlation matrix is then obtained by dividing each entry of the covariance matrix by σ_y^2, the variance of spatial average of permeability. The correlation matrix is included in Fig. 3.2.

(d) Sensitivity matrix of the basic model

For the idealized 1-D model, nodal heads (h_j) can be expressed in terms of element permeabilities (k_i) as follows:

$$h_j = h_o - \frac{h_o - h_m}{\left(\frac{1}{k_1} + \frac{1}{k_2} + \cdots + \frac{1}{k_m}\right)} \left(\frac{1}{k_1} + \frac{1}{k_2} + \cdots + \frac{1}{k_j}\right) \quad (3.1)$$

Exact derivation of Eq. 3.1 is included in the appendix. Upstream and downstream heads are h_o and h_m respectively, and m is the number of discretized units.

Eq. 3.1 reveals three important characteristics of the 1-D model. (a) First of all, it shows that hydraulic head is independent of the mean permeability. As long as the ratios of all the k_is remain constant, the h_js will remain the same. (b) Equally important is that h_j is much more linear in terms of the resistivity, $1/k_i$, than in terms of the permeability, k_i. Therefore, the linearity can be taken advantage of by formulating the sensitivity matrix in terms of the resistivity instead of the permeability. (c) Eq. 3.1 also indicates that as m, the number of elements, increases,

the denominator $(1/k_1 + 1/k_2 + 1/k_3 + \cdots 1/k_m)$ becomes less dependent on any particular permeability, k_i. As a result, h_j becomes increasingly linear in terms of $1/k_i$ as m increases.

It is possible to differentiate Eq. 3.1 and obtain the instantaneous slope $\partial h_j/\partial(1/k_i)$:

$$\frac{\partial h_j}{\partial \frac{1}{k_i}} = (h_o - h_m)\left(\frac{1}{k_1} + \frac{1}{k_2} + \cdots \frac{1}{k_m}\right)^{-1}\left[\left(\frac{1}{k_1} + \frac{1}{k_2} + \cdots \frac{1}{k_m}\right)^{-1}\right.$$

$$\left.\left(\frac{1}{k_1} + \frac{1}{k_2} + \cdots \frac{1}{k_j}\right) - 1\right] \quad \text{for } 1 \leq i \leq j$$

or (3.2)

$$\frac{\partial h_j}{\partial \frac{1}{k_i}} = (h_o - h_m)\left(\frac{1}{k_1} + \frac{1}{k_2} + \cdots \frac{1}{k_m}\right)^{-2}\left(\frac{1}{k_1} + \frac{1}{k_2} + \cdots \frac{1}{k_j}\right)$$

$$\text{for } j < i \leq m$$

$\partial h_j/\partial(1/k_i)$ can be assembled into the sensitivity matrix $\underline{A}$. Now that the sensitivity matrix is formulated in terms of the resistivity, Eq. 2.9 has to undergo some minor modifications. σ_y^2 in Eq. 2.9 has to be replaced by σ_z^2, which is the variance of spatial average of resistivity. Scale of fluctuation of the resistivity, $\theta_{1/k}$, can be taken as equal to the scale of fluctuation of permeability, θ_k. The correlation matrix, $\underline{C}_{1/k}$ and variance reduction factor, $\Gamma^2_{1/k}$, for resistivity are identical to those for permeability. Thus, Eq. 2.9 can be rewritten as:

$$\underline{\Sigma}_h = \sigma_z^2 \, \underline{A} \, \underline{C}_{1/k} \, \underline{A}^T \tag{3.3}$$

Alternatively, the sensitivity matrix can be derived using the FEDAR program mentioned in Chapter II. There are two reasons why it is important to go through the trouble of calculating the approximate slope when the exact slope can be obtained analytically. First of all, the instantaneous slope may not be the best representation of the average behavior of the system. Secondly, simple analytical counterpart of Eq. 3.1 cannot be worked out for more complicated underseepage models. Formulation of sensitivity matrices for such cases will be fully dependent on The FEDAR program. It is, therefore, very important to understand the mechanics of the program starting from a simple 1-D case.

For linear functions, the sensitivity matrix obtained should be independent of the permeability increments used in the FEDAR program. Because of the nonlinearity of Eq. 3.1, different sensitivity matrices for different permeability increments are obtained. However, all the sensitivity matrices obtained have structures identical to the sensitivity matrix derived analytically. They only differ from one another by constant factors. These factors are defined here as the variability coefficients which express the ratios of the values in a sensitivity matrix for any Δk to the corresponding values in the sensitivity matrix for a reference Δk. The variability coefficient is 1.0 if the relationship between nodal heads and element permeability is linear.

In Fig. 3.3, the variability coefficient for sensitivity matrix formulated based on the resistivity over a range of different permeability increments is plotted against $\log(k(1+\Delta k))$, using a reference increment $\Delta k = 50\%$[1]. Within the $\pm 1\sigma$ range, the variability coefficient ranges from

[1] The choice of $\Delta k = 50\%$ as the reference increment is arbitrary. The instantaneous sensitivity matrix, $\Delta k = 0\%$, is not chosen because in most cases, analytical derivation of instantaneous slope is very difficult, if not impossible.

0.88 to 1.01. An average value of 0.95 was used to correct for the sensitivity matrix for Δk = 50%, and the resulting sensitivity matrix is presented in Fig. 3.4.

Variability coefficient, as defined above, gives an indication of the linearity of the function we are dealing with. In Eq. 3.1, we observed that h is a more nonlinear function of permeability than resistivity. The variability coefficient calculated for sensitivity matrix defined in terms of $\partial h_j/\partial k_i$ as shown in Fig. 3.3 confirmed the observation. Over the $\pm 1\sigma$ range, the variability coefficients now varies over a wider range (from 0.85 to 2.39). Fig. 3.3 also shows the variation of the variability coefficient for sensitivity matrix defined in terms of $\partial h_j/\partial \log k_i$.

3.2 Results from 1-D Underseepage Study

The following sections will present results from parametric study of 1-D underseepage behavior. FOSM prediction of σ_h for the basic model is presented in Fig. 3.5[1]. Maximum uncertainty for nodal heads occurs at the middle of the underseepage path. The uncertainty drops to zero at the two ends because the boundary nodal heads are fixed at 100' and 0'. Since σ_h is symmetrical with respect to the middle of the underseepage path, subsequent results will only be presented for one half of the underseepage path.

(a) Effect of varying number of discretized units.

The basic model has ten discretized units. This section will examine whether or not this type of discretization is adequate.

First of all, Fig. 3.6 is a plot similar to Fig. 3.3 showing the effect

---

[1] The reader is reminded that σ_h is the standard deviation for head and not the horizontal stress.

of different numbers of discretized units on the variability coefficient. As the number of elements increases, linearity increases such that when the underseepage path is discretized into forty elements, the variability coefficient over the $\pm 1\sigma$ range is essentially constant. The result here is consistent with what was observed in Equation 3.1.

Table 3.1 compares the σ_h predicted by using different degree of discretization. Average variability coefficient over the $\pm 1\sigma$ range has been used in each of the cases as a correction for the sensitivity matrix obtained for $\Delta k = 50\%$. The table shows that σ_h predicted separately by the ten and by the forty element underseepage models agree very well (maximum discrepancy is less than 2%). Even the five element underseepage model yields σ_h which are only at a maximum of 1% off from σ_h obtained for the ten element model. Hence, we can conclude that the FOSM approach is not sensitive to the degree of discretization. FOSM approach is regarded as being a computationally efficient method of studying the underseepage problem since we only need a minimal amount of discretization to ensure the convergence of σ_h.

The FOSM is insensitive to discretization because of the use of the variance reduction factor, $\Gamma^2(\tau)$, in its basic methodology. The variance reduction factor was not accounted for by Freeze (1975). Consequently, Freeze's Monte Carlo simulation approach produced σ_h predictions which depend on the number of discretized units.

Obviously, the concept of representative elementary volume (REV) by Bear (1972) is irrelevant to this study, since discretization is not a problem here. General experience with the 1-D model indicates that the results from FOSM analysis are reliable as long as the scale of fluctuation

is at least half the size of an element. That explains why for this five element case, when θ = 225', a fairly good estimate of σ_h is still obtainable.

(b) Effect of totally uncorrelated blocks

Freeze (1975) used Monte Carlo simulation on a 1-D model consisting of a series of totally uncorrelated blocks to study head uncertainty. His assumption of totally uncorrelated blocks neglects spatial correlation of permeability which is unrealistic in simulating 1-D seepage behavior because σ_h will decrease as the number of blocks increases.

In this section, we will study head uncertainty under an assumed model consisting of totally uncorrelated blocks. The purpose is to check the reliability of FOSM approach by comparing the FOSM result for this model with Freeze's result.

The correlation matrix in this situation is an identity matrix with the diagonal terms being equal to unity and all other entries being zero. Eq. 3.3 can be rewritten as:

$$\underline{\Sigma}_h = \sigma_z^2 \, \underline{A} \, \underline{A}^T$$

To be consistent with Freeze's appraoch, σ_z^2 will have to be the point variance of the resistivity, 1/k (i.e., no variance reduction due to spatail averaging). The sensitivity matrix will remain the same.

σ_h calculated for the model is tabulated in Table 3.2. Freeze's Monte Carlo simulation result is also tabulated.

The discrepancy between Freeze's result and the FOSM result is only about 5%. This indicates that the FOSM approach is a reliable approach for obtaining σ_h. It is not possible to determine which of the two

approaches yields a better estimate of σ_h for this situation. The 5% disagreement is probably due to the fact that both approaches are only numerical approximations which are not theoretically exact.

(c) Effect of varying scale of fluctuation

The scale of fluctuation, 225', chosen for the basic model is within the range for deposits which can be considered to have long scales of fluctuation. It may typify deposits, such as lacustrine soil, whose point permeability fluctuates slowly about its mean. On the contrary, foundations that are composed of glacial till or fluvial deposit tend to have smaller scales of fluctuation. Soils deposited by river action, for example, vary in size and porosity according to the velocity of water which fluctuates a lot both locally and seasonally. This type of deposit will have a smaller scale of fluctuation becase of the highly fluctuating coefficient of permeability.

Table 3.3 summarizes the result obtained by varying the scale of fluctuation of the basic model. Maximum uncertainty occurs when θ is about 250', which is exactly one half of the underseepage length. When θ is small compared to the underseepage length, all the element permeabilities are almost independent of one another. The chance of finding an element with high permeability adjacent to another one with high permeability is very low. Variance reduction due to spatial averaging for small θ is high. Therefore, when θ is small, σ_h is very small. As θ increases, σ_h increases because of the increased correlation between adjacent elements. However, as θ exceeds one half of the underseepage length, the effect of finite boundaries becomes important. σ_h begins to decrease with increasing θ and it decays back to zero as θ becomes very very large.

Table 3.4 compares Dettinger's (1979) results with the results from the present study of similar cases. Dettinger had assumed that the spatial correlation for permeability can be represented by a simple exponential correlation function. The correlation lengths (ℓ) for his function are 100' and 200' for the results tabulated. These lengths are equivalent to scales of fluctuation of 200' and 400' (Eq. 2.4).

At θ = 200, Table 3.4 shows that there is a 10-25% disagreement between Dettinger's results and the results from the present study. The discrepancy arises because of the use of different correlation functions to describe spatial correlation. Fig. 2.2 shows that $\Gamma(T)$ for simple exponential correlation function is about 10% higher than $\Gamma(T)$ for triangular correlation function when T is equal to θ. The discrepancy between the two results becomes significantly smaller if the above differences in the correlation function are taken into account.

Dettinger also noticed the same increase then decrease in σ_h with increasing θ. However, his maximum uncertainty for the same model occurs at a higher θ than the present study. Table 3.4 shows that Dettinger obtained higher σ_h for θ = 400' than for θ = 200'. This disagreement can again be explained by the differences in the correlation functions used. At θ = 400, the ratio T/θ is 0.125. Fig. 2.2 shows that at T/θ = 0.125, $\Gamma(T)$ for both correlation functions are both equal to 1.0 approximately. When θ = 200, T/θ becomes 0.25, and $\Gamma(T)$ from simple exponential correlation function is about 10% lower than $\Gamma(T)$ for triangular correlation function. From the above discussion, one can expect a shift towards higher θ for maximum uncertainty when simple exponential correlation function is used. Therefore, the results from present study is consistent with Dettinger's results.

The output correlation function of piezometric heads for the basic model is plotted in Fig. 3.7. The output correlation function does not have a nice triangular shape and its scale of fluctuation is higher than the input scale of fluctuation of permeability. Output θ_h for different input θ_k are tabulated in Table 3.5. No conclusive relationship between θ_h and θ_k is observed except that θ_h is consistently larger than θ_k, and that θ_h increases less rapidly than θ_k.

(d) Effect of having very small scale of fluctuation (constant head uncertainty)

It was mentioned in Chapter II that several investigators had studied the flow of water through a statistically homogeneous media by analytical procedures. Each analytical solution relates the variability of head to the variability of permeability under a set of imposed conditions. One of the major assumptions that an analytical solution invokes is that the boundaries are sufficiently far away from the point concerned so that a constant head uncertainty is achieved. Previous sections have shown that boundary effect plays an important role in reducing head uncertainty. This section will focus on the question of whether constant head uncertainty is important for dams.

Fig. 3.8 compares the normalized σ_h profiles for θ = 225' and θ = 30'. As θ is reduced, the peak of σ_h profile is flattened. For θ = 30', σ_h is almost constant from x = 200 to 300'. One can expect to obtain essentially constant σ_h as the ratio of θ to underseepage length becomes very very small.

However, we know from Section 3.2(d) that when θ/L is very small, σ_h becomes insignificantly small also. Therefore, σ_h from analytical solutions

cannot be applied to dams because of the effect of finite boundaries. This is not to dispute the validity of results obtained from analytical means. Such kind of constant head uncertainty is more useful for the study of seepage uncertainty in aquifers whose boundaries are indeed very far apart.

(e) Effect of forumlating $\underline{A}$ based on log k instead of 1/k

Eq. 3.1 indicates that h is approximately linear in 1/k as the number of elements increases. That is why the formulation of sensitivity matrix $\underline{A}$ has been based on 1/k. To ensure the general applicability of the FOSM formulation in dealing with seepage uncertainty, we have to make sure that the method will yield equally consistent results for reasonably nonlinear functions. Seepage through real dam is very complicated and cannot be represented by simple block structure such as the basic model. It is not hard to spell out situations where h is no longer linear in terms of 1/k.

In this section, we will investigate the effect of linearization of the functional relationship between h and log k on the outcome of the analysis. Fig. 3.9(a) is a plot similar to Fig. 3.3. As the number of elements increases, $\underline{A}$ does not become increasingly linear. Instead, the variability coefficient approaches asymptotically to an exponential relationship approximated by the line for forty elements in Fig. 3.9(a).

It turns out that the best way to correct for the nonlinearity is to use the equivalent slope method. Since k is assumed to be lognormally distributed, a weighted average of the variability coefficient (based on the probability distribution) can be calculated. The weighted average is then applied as a correction to the sensitivity matrix obtained for the reference increment. The procedure is shown in Fig. 3.9(b).

σ_h obtained by using $\underline{A}$ formulated based on log k is tabulated in Table 3.6. The σ_h predicted agrees very well with σ_h in Fig. 3.5. This shows that FOSM works well even for functions which are fairly nonlinear provided the sensitivity matrix is corrected for its nonlinearity.

(f) Effect of using higher variance for permeability

$\sigma_{\log k}$ for the basic model is 0.25. Realistic values for $\sigma_{\log k}$ range from 0.20 to 1.50 (Freeze 1975). So, the $\sigma_{\log k}$ used in this study is in the low range.

The same methodology could have been applied to a medium with higher $\sigma_{\log k}$. The only problem with that is that the behavior of the basic underseepage model becomes increasingly nonlinear for higher values of $\sigma_{\log k}$. One can compensate the nonlinearity by increasing the number of discretized units. The main reason why higher number of elements and more realistic $\sigma_{\log k}$ is not used for the basic model is because the intention of this chapter is to bring out the characteristics of 1-D underseepage while keeping the problem as simple as possible.

Another related question is what would happen to σ_h if the mean of k is different from the basic model. This would depend on how σ_k varies with m_k. If σ_k is constant regardless of m_k, then σ_h will be inversely proportional to m_k. On the other hand, if $\sigma_{\log k}$ can be assumed to remain constant regardless of m_k (Willardson and Hurst 1965), then σ_h will be the same as what is predicted. Actual soil will behave in between the two bounds stated above.

3.3 Limitations of 1-D Underseepage Model

σ_h obtained in this chapter is only valid for steady state seepage condition. Transient response is assumed to be unimportant in this study. For most large dams, the water level is relatively constant, so the effect of variable water elevation on steady state piezometric head can be ignored. If transient time to steady state seepage of one year is reasonable, then the results are only valid for foundations whose average permeablilities are on the order of 10^{-5} ft/sec or more. This minimum permeability limit has to be raised if one is dealing with a dam with fluctuating water level.

An approach such as Schmidheini's (1978) can be developed to account for the transient behavior. the present study, however, will not concern itself with transient behavior of seepage.

For reasons which will become obvious in Chapter IV, the results in the chapter should be treated as the upperbound solution for σ_h. The intention of this chapter is to study the general applicability and limitations of the basic methodology through the use of a simplified underseepage model. 1-D model was chosen because of the availability of published results for comparison purposes. The study of this chapter is not an end to itself. It serves as the foundation for subsequent chapters which will deal with more realistic models.

3.4 Conclusions

Major conclusions for this chapter are as follows:

(a) FOSM approach is a good approach for studying seepage behavior. 1-D results obtained by FOSM approach agree with what was obtained by Freeze (1975) and Dettinger (1979).

(b) Important factors governing σ_h and its distribution along the underseepage path are: θ/L, ratio of scale of fluctuation to underseepage length; σ_k^2, variance of permeability; and $\underline{A}$, sensitivity of h to change in k.

(c) Despite the fact that FOSM approach is only an approximate technique, consistent results were obtained even for fairly non linear functions if the non linearity is corrected by using the technique proposed in Section 3.2(e).

(d) For the 1-D underseepage model, h is approximately linear in terms of 1/k. The linearity increases as m, the number of discretized units, increases.

(e) Sensitivity matrix, $\underline{A}$, can be reliably obtained by the FEDAR program described in Chapter II.

(f) Because of the influence of finite boundaries, analytical solutions of σ_h should not be applied to dams.

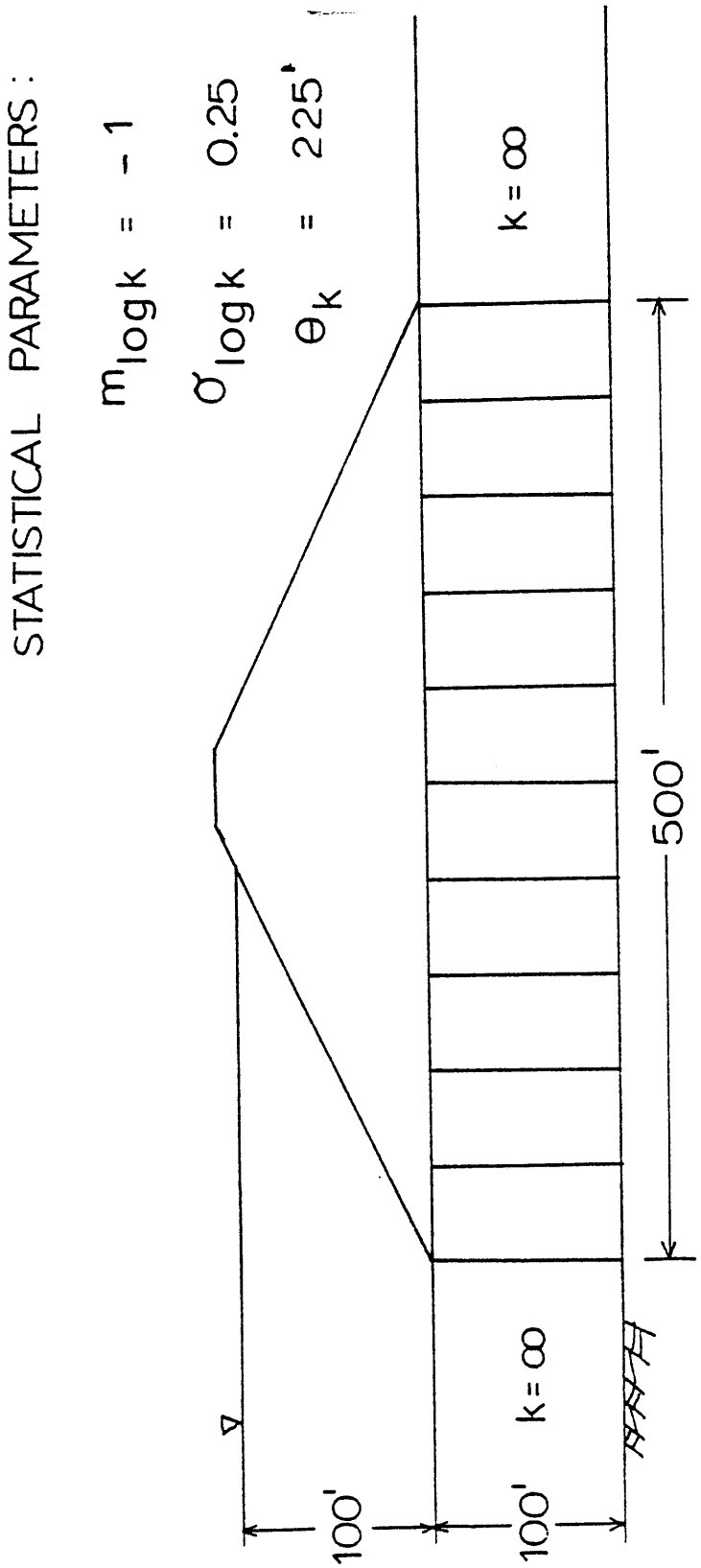

FIG. 3.1 BASIC 1D UNDERSEEPAGE MODEL

1.000	0.840	0.600	0.360	0.125	0.005	0.000	0.000	0.000	0.000
0.840	1.000	0.840	0.600	0.360	0.125	0.005	0.000	0.000	0.000
0.600	0.840	1.000	0.840	0.600	0.360	0.125	0.005	0.000	0.000
0.360	0.600	0.840	1.000	0.840	0.600	0.360	0.125	0.005	0.000
0.125	0.360	0.600	0.840	1.000	0.840	0.600	0.360	0.125	0.005
0.005	0.125	00360	0.600	0.840	1.000	0.840	0.600	0.360	0.125
0.000	0.005	0.125	0.360	0.600	0.840	1.000	0.840	0.600	0.360
0.000	0.000	0.005	0.125	0.360	0.600	0.840	1.000	0.840	0.600
0.000	0.000	0.000	0.005	0.125	0.360	0.600	0.840	1.000	0.840
0.000	0.000	0.000	0.000	0.005	0.125	0.360	0.600	0.840	1.000

FIG. 3.2 CORRELATION MATRIX FOR PERMEABILITY OF THE BASIC MODEL

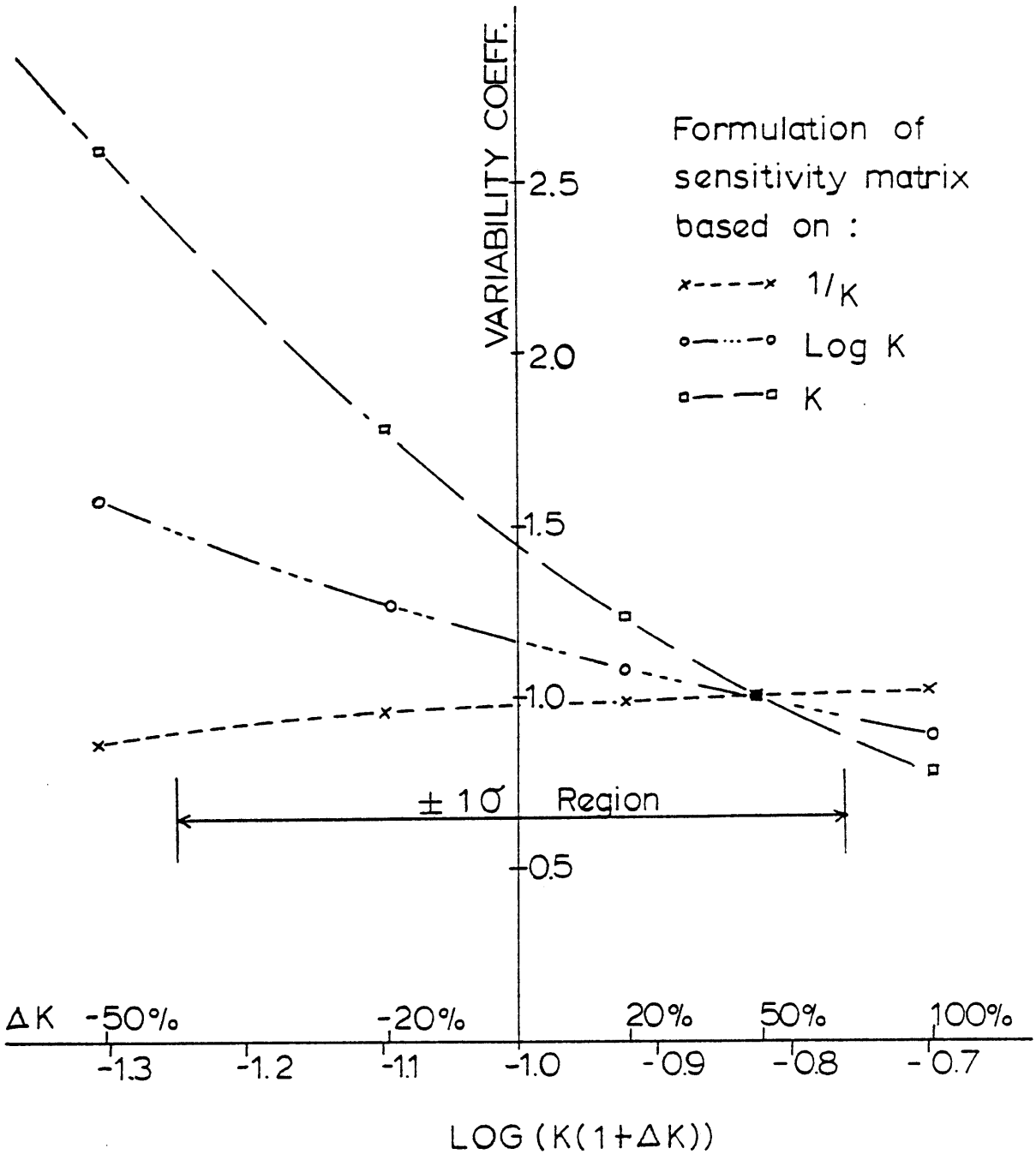

FIG. 3.3 PLOT OF VARIABILITY COEFFICIENTS VS. LOG(K(1+ΔK))

0.000	0.000	0.000	0.000	0.000	0.000	0.000	0.000	0.000	0.000
-0.885	0.098	0.098	0.098	0.098	0.098	0.098	0.098	0.098	0.098
-0.787	-0.787	0.197	0.197	0.197	0.197	0.197	0.197	0.197	0.197
-0.688	-0.688	-0.688	0.295	0.295	0.295	0.295	0.295	0.295	0.295
-0.590	-0.590	-0.590	-0.590	0.393	0.393	0.393	0.393	0.393	0.393
-0.491	-0.491	-0.491	-0.491	-0.491	0.491	0.491	0.491	0.491	0.491
-0.393	-0.393	-0.393	-0.393	-0.393	-0.393	0.590	0.590	0.590	0.590
-0.295	-0.295	-0.295	-0.295	-0.295	-0.295	-0.295	0.688	0.688	0.688
-0.197	-0.197	-0.197	-0.197	-0.197	-0.197	-0.197	-0.197	0.787	0.787
-0.098	-0.098	-0.098	-0.098	-0.098	-0.098	-0.098	-0.098	-0.098	0.885
0.000	0.000	0.000	0.000	0.000	0.000	0.000	0.000	0.000	0.000

FIG. 3.4 SENSITIVITY MATRIX FOR THE BASIC 1-D MODEL

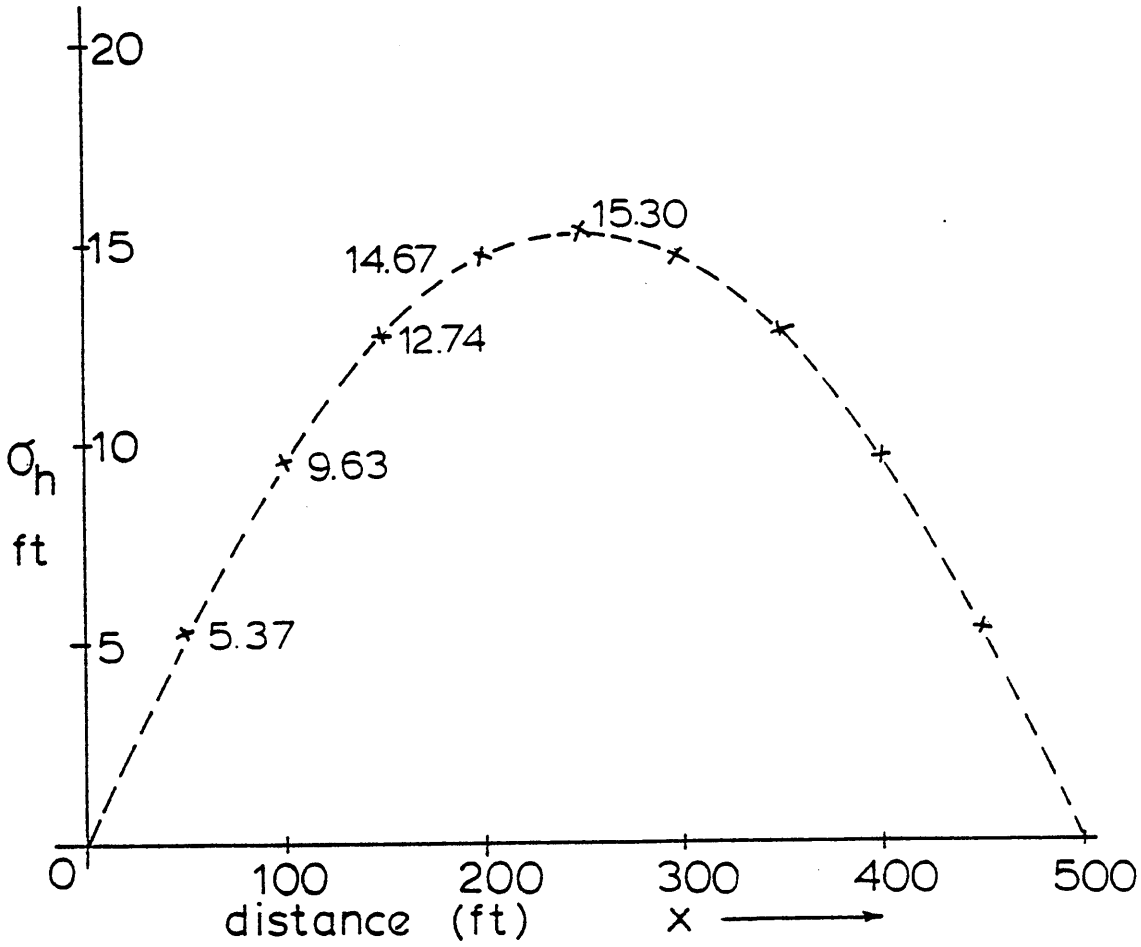

FIG. 3.5 σ_h PROFILE FOR THE BASIC 1D MODEL

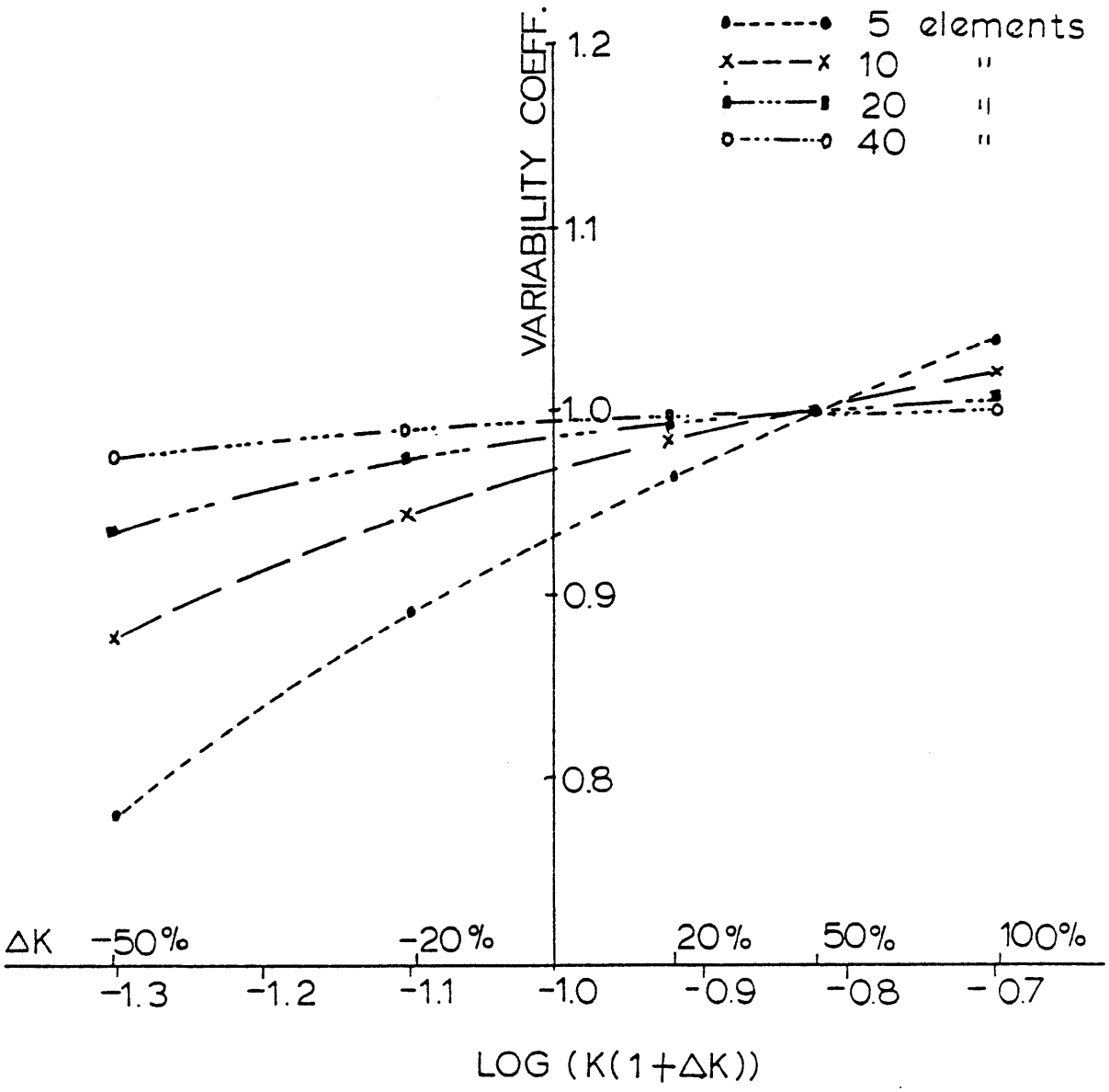

FIG. 3.6 PLOT OF VARIABILITY COEFFICIENTS FOR DIFFERENT NUMBER OF ELEMENTS

DISTANCES (FT)[i]	0	50	100	150	200	250
5 ELEMENTS	0.00	[ii]	9.56	[ii]	14.54	[ii]
10 ELEMENTS	0.00	5.37	9.63	12.74	14.67	15.30
20 ELEMENTS	0.00	5.44	9.74	12.88	14.78	15.43
40 ELEMENTS	0.00	5.46	9.78	12.95	14.89	15.54

TABLE 3.1 Comparison of σ_h obtained for different degrees of discretization

notes: i only one half of the underseepage path is considered because of symmetry
ii results are unavailable because there are only 5 elements

DISTANCES (FT)	0	50	100	150	200	250
FOSM	0.00	5.84	7.79	8.92	9.53	9.72
FREEZE (1975)	0.00	5.2	7.1	8.1	8.9	9.1

TABLE 3.2 Comparison of σ_h obtained by FOSM with σ_h obtained by Freeze (for totally uncorrelated blocks)

DISTANCES (FT)	0	50	100	150	200	250
θ = 30 ft	0.00	4.04	5.69	6.64	7.15	7.30
θ = 90 ft	0.00	5.23	8.65	10.52	11.52	11.82
θ = 150 ft	0.00	5.40	9.48	12.19	13.66	14.09
θ = 225 ft	0.00	5.38	9.65	12.74	14.67	15.30
θ = 250 ft	0.00	5.34	9.61	12.74	14.71	15.38
θ = 275 ft	0.00	5.30	9.56	12.68	14.65	15.31
θ = 300 ft	0.00	5.25	9.47	12.56	14.50	15.13
θ = 400 ft	0.00	4.95	8.88	11.68	13.38	13.93
θ = 500 ft	0.00	4.52	8.04	10.55	12.07	12.56

TABLE 3.3 Comparison of σ_h at different scales of fluctuation, θ

DISTANCES (FT)		0	50	100	150	200	250
FROM	θ = 225 ft	0.00	5.38	9.65	12.74	14.67	15.30
TABLE 3.3	θ = 400 ft	0.00	4.95	8.88	11.68	13.38	13.93
FROM	θ = 200 ft	0.00	5.4	8.4	10.4	11.0	11.5
DETTINGER (1979)	θ = 400 ft	0.00	5.4	8.6	11.0	12.4	12.8

TABLE 3.4 Comparison of results with Dettinger (1979)

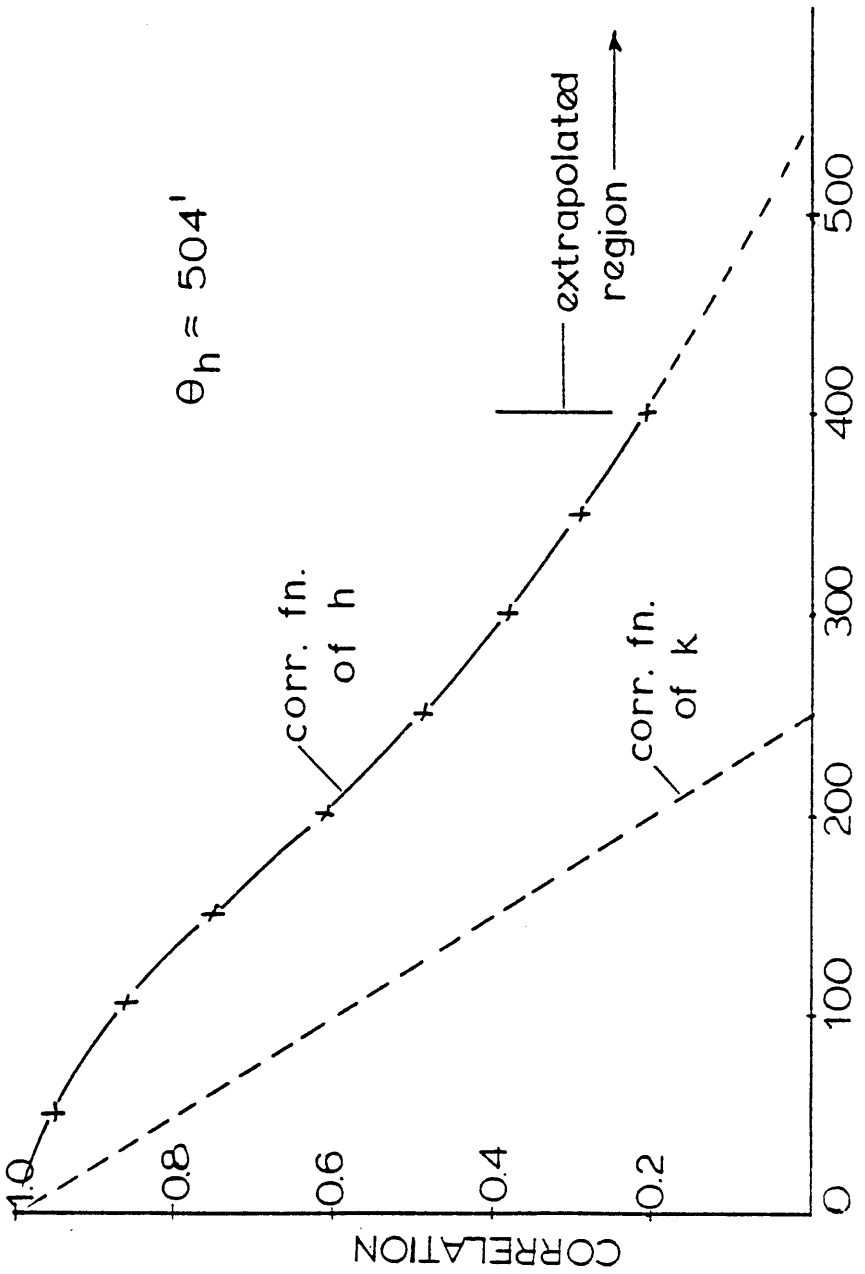

FIG. 3.7 CORRELATION FUNCTION OF h FOR $\theta_k = 225'$

θ_k	θ_h
90'	376'
225'	504'
400'	712'

TABLE 3.5 Comparison of θ_k vs θ_h

DISTANCES (FT)	0	50	100	150	200	250
$\sigma_{h_{1/k}}$	0.00	5.37	9.63	12.74	14.67	15.30
$\sigma_{h_{\log k}}$	0.00	5.22	9.36	12.38	14.26	14.87

TABLE 3.6 Comparison of σ_h obtained by formulating the sensitivity matrix based on logk instead of 1/k

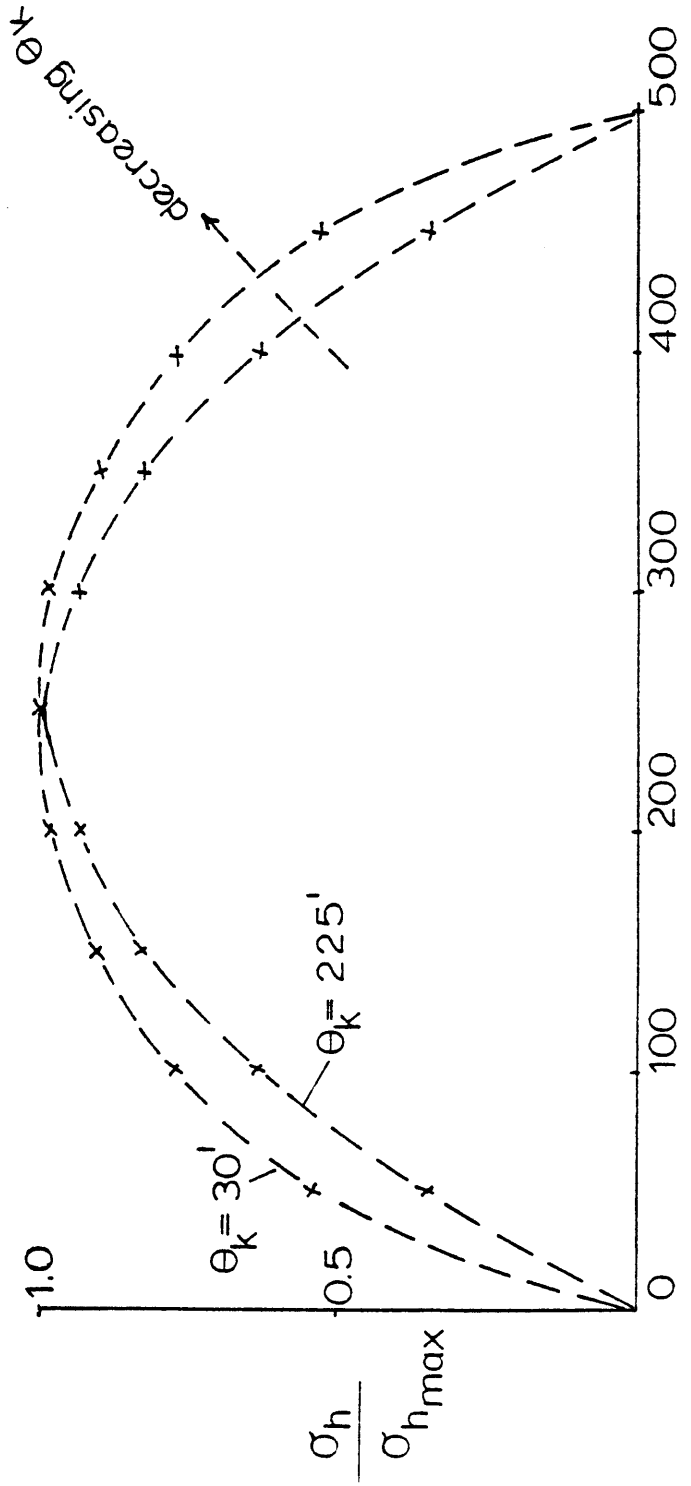

FIG. 3.8 NORMALIZED σ_h PROFILES FOR $\theta = 225'$ AND $\theta = 30'$

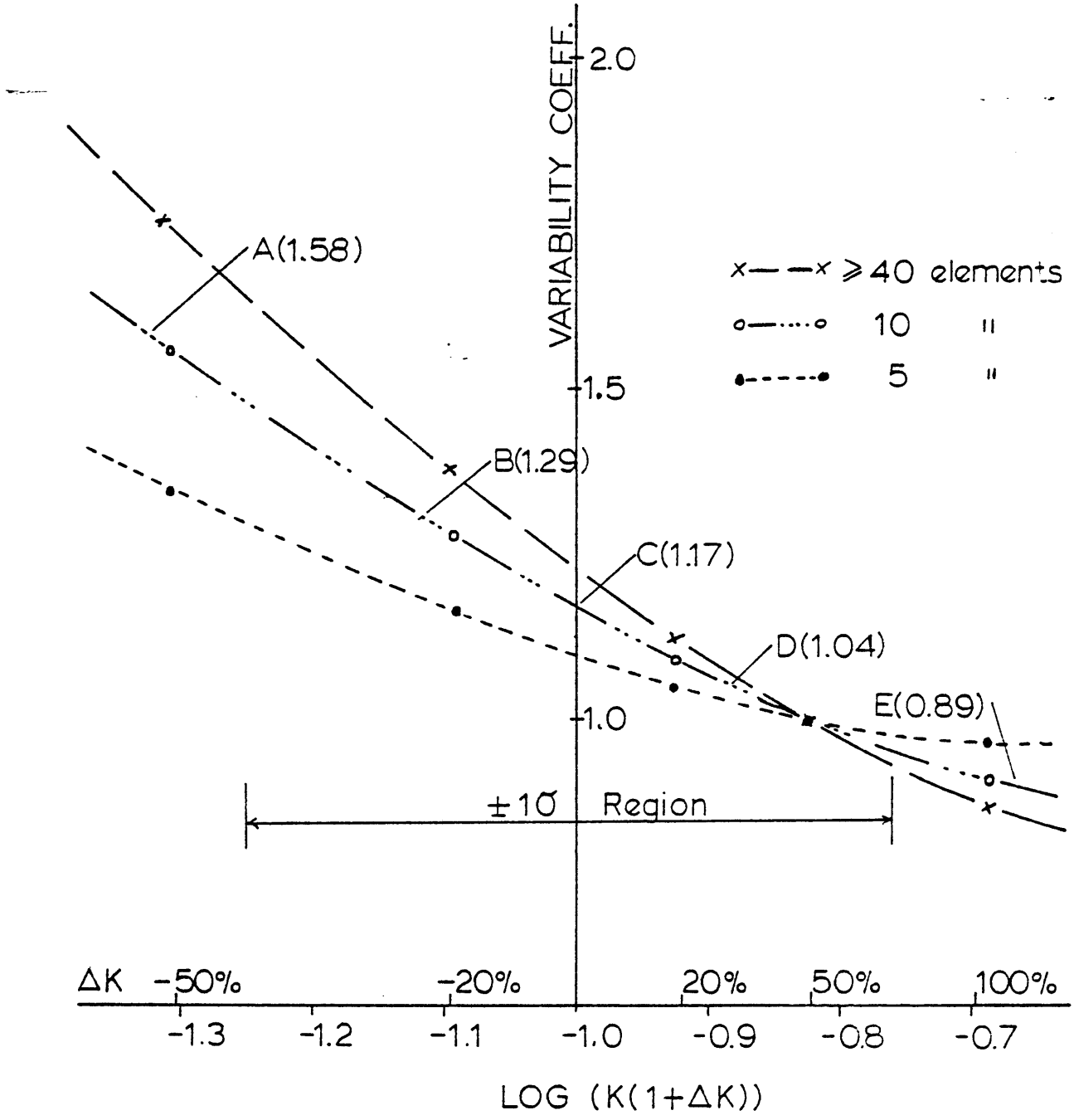

FIG. 3.9a VARIABILITY COEFFICIENTS FOR SENSITIVITY MATRICES FORMULATED BASED ON LOG K

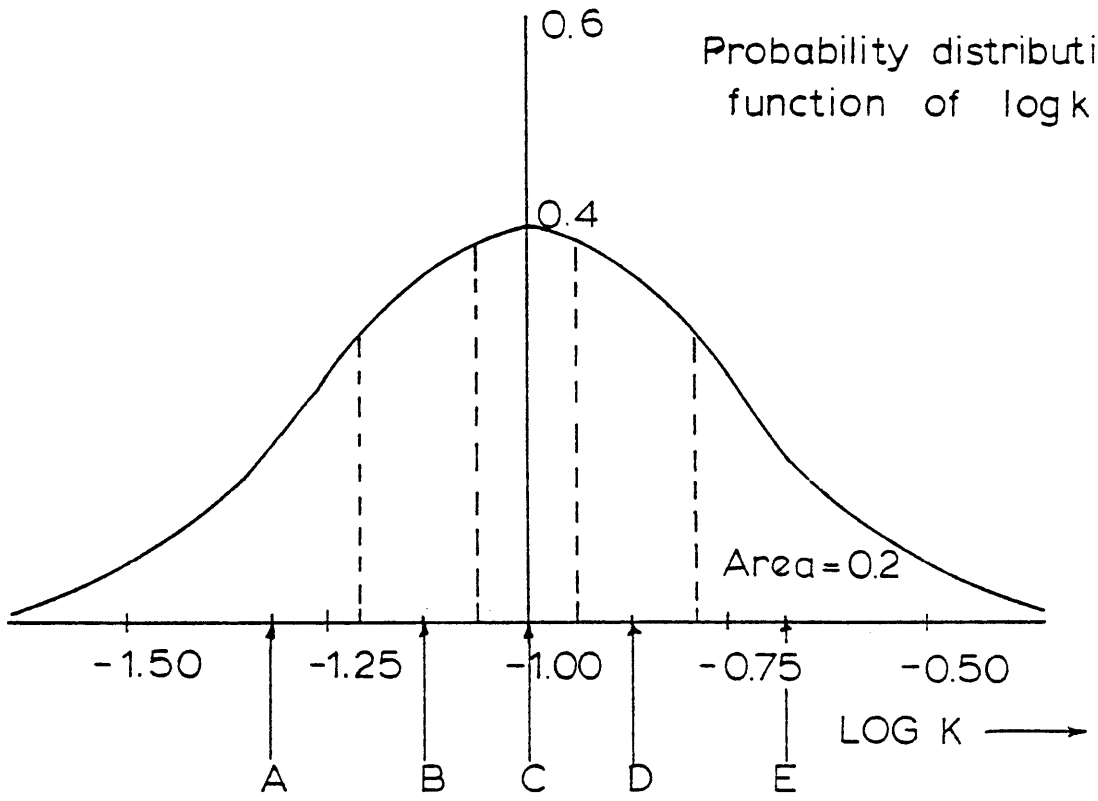

POINTS	V.C. (from fig. 3.9a)
A	1.58
B	1.30
C	1.17
D	1.04
E	0.98

$5.98 \times 0.2 = 1.196$ — Correction factor for $\Delta k = 50\%$

FIG. 3.9b EQUIVALENT SLOPE METHOD FOR CORRECTING NONLINEARITY

CHAPTER IV TWO-DIMENSIONAL UNDERSEEPAGE STUDY

Realistic representation of the underseepage behavior can not be achieved by using the 1-D model discussed in Chapter III. In this chapter, a two-dimensional model will be used. It differs from the 1-D model in that it permits variation of permeability in the vertical direction. Nonhomogeneity of permeability in the vertical direction will inevitably induce flow in the direction transverse to the mean flow, thus creating a flow situation which is significantly different from the 1-D case.

This chapter is developed along the same line as Chapter III. First, a basic 2-D model is described. Included in the first part is a discussion of the procedure by which the FOSM methodology in Chapter II can be extended for use in a 2-D study. Parametric study on the 2-D model is then carried out to study the influence of different factors on σ_h. At the same time, frequent comparison between the behavior of the 2-D model and its 1-D counterpart is made. Finally, the strengths as well as the limitations of the 2-D underseepage model are discussed.

4.1 Basic 2-D Model

(a) Geometry of the basic model

Fig. 4.1 shows the underseepage path of a typical dam. The dimension of the underseepage path is exactly the same as in the 1-D case except that now, each vertical section consists of five elements rather than one. Again, all the elements are chosen to be equal in size to preserve statistical homogeneity when dealing with spatial averages.

The mean flow path of the 2-D model will remain one dimensional. However, unlike the 1-D model, the 2-D model permits freedom of flow in

the vertical direction in case it becomes necessary to circumvent an obstacle of low permeability or to "short cut" through an element with high permeability. This is consistent with the concept of "path of minimum resistance" that characterizes seepage of water. This type of flexibility is unavailable in a 1-D model. Water is forced to seep through every element along its mean flow path, regardless of the permeability of the element. The flow is artificial and greatly susceptible to local variability of the permeability. Therefore, σ_h from a 1-D model should be expected to be higher than σ_h from a 2-D model.

(b) Statistical parameters of the basic model

It is no longer sufficient to describe a 2-D model only by three statistical parameters. Equally important are the parameters in the vertical direction. A total of six parameters will now be considered: m_{k_x}, m_{k_y}, $\sigma^2_{k_y}$, θ^x_k and θ^y_k. We also have to account for possible interdependence between the statistical parameters in the vertical and horizontal directions.

Unlike the 1-D case, we are now dealing with spatial averages over rectangular elements. In Chapter II, we saw that for the 1-D case, the point variance of permeability has to be multiplied by a factor Γ^2_k to obtain the variance for a spatial average. Γ^2_k accounts for variance reduction due to spatial averaging over an interval consisting of random variables that are not fully correlated. Similarly, for the 2-D case, we have to use a 2-D variance function $\Gamma^2_k(x,y)$ to take care of the variance reduction in the x and y directions.

Vanmarcke (1979b) showed that the 2-D variance function can be expressed as follows:

$$\Gamma^2(U,V) = \Gamma^2(U) \times \Gamma^2(V|U) \qquad (4.1)$$

U and V are the lengths of the rectangular area in the x and y directions respectively. $\Gamma^2(U)$ is simply the variance function in the x direction. It can have the same form as the 1-D variance function. Its averaging interval is U, and its scale of fluctuation is θ_k^x. $\Gamma^2(V|U)$ is the conditional variance function in the y direction. It can also have the same form as the 1-D variance function. Its averaging interval is V, but its scale of fluctuation is $\theta_{k|U}^y$, the "conditional" scale of fluctuation, instead of θ_k^y.

$\theta_{k|U}^y$ can vary anywhere between θ_k^y to $n\theta_k^y$ depending on the averaging distance, U, in the x direction. Averaging in the x direction has the net effect of increasing the scale of fluctuation in the y direction. For any 2-D correlation function, the limiting value, n, is defined as

$$n = \frac{\alpha_k}{\theta_k^{x^2}} \qquad (4.2)$$

In Equation 4.2, θ_k^x is the scale of fluctuation in the x direction, and α_k is the volume underneath the 2-D correlation function, $\rho_k(r)$:

$$\alpha_k = 2\pi \int_0^\infty r\, \rho_k(r)dr \qquad (4.3)$$

The value of $\theta_{k|U}^y$ can be obtained by multiplying θ_k^y by a factor C, which is a function of the quantity U/θ_k^x.

$$\theta^{y}_{k|U} = \theta^{y}_{k} \times C(U/\theta^{x}_{k}) \tag{4.4}$$

C is the characteristic of a 2-D correlation function. Fig. 4.2 is a typical plot of C versus U/θ^{x}_{k}. C increases with U/θ^{x}_{k} until it reaches the asymptotic limit, n. For most 2-D correlation functions, n varies from 1.0 to 1.5.

The 2-D variance is commutative. $\Gamma^2(U,V)$ is exactly the same as $\Gamma^2(V,U)$. $\Gamma^2(V,U)$ is simply the variance function obtained by considering the y direction first.

$$\Gamma^2(V,U) = \Gamma^2(V) \times \Gamma^2(U|V) \tag{4.5}$$

A rather simplistic set of statistical parameters has been chosen for the 2-D basic model. The basic model is assumed to be statistically homogeneous and isotropic. The means of log k in both directions, $m_{\log k_x}$ and $m_{\log k_y}$, are equal to -1.0, the same as the 1-D basic model. Their standard deviations, $\sigma_{\log k_x}$ and $\sigma_{\log k_y}$, are equal to 0.25. The scales of fluctuation, θ^{x}_{k} and θ^{y}_{k}, for the basic model are both equal to 225'. Also, for simplicity, the correlation function chosen for the 2-D study has no coupling between the two directions. This implies that n in Eq. 4.2 is equal to 1.0. The triangular correlation function will be used in both directions. Because of the assumption that there is no coupling between the two directions, Eq. 4.1 can be rewritten as:

$$\Gamma^2(U,V) = \Gamma^2(U) \times \Gamma^2(V) \tag{4.6}$$

where Γ^2 is the variance function defined in Eq. 2.6.

(c) Correlation matrix of the basic model

Vanmarcke (1979b) derived the correlation between the spatial averages over two rectangular elements as:

$$\rho[y_{U_1V_1}, y_{U_2V_2}] = \frac{1}{4U_1V_1U_2V_2\ \Gamma(U_1V_1)\ \Gamma(U_2V_2)} \sum_{i=0}^{3}\sum_{j=0}^{3} (-1)^{i+j}\ U_i^* V_j^*\ \Gamma^2(U_i^*, V_j^*) \tag{4.7}$$

Eq. 4.7 is a direct extension of Eq. 2.7 for the 1-D case. Fig. 4.3 illustrates the meaning of the symbols used in Eq. 4.7. $y_{U_1V_1}$ is the spatial average over a rectangular element whose sides are U_1 and V_1 in length.

A fundamental 5 x 10 correlation matrix can be derived for the basic model. The fundamental correlation matrix for $\theta_k^x = 225'$ and $\theta_k^y = 225'$ is included in Fig. 4.4. It contains all the numbers necessary to make up the larger 50 x 50 correlation matrix. Element ij of the fundamental correlation matrix is the correlation between the spatial averages of two rectangles U x (j-1) feet apart horizontally and V x (i-1) feet apart vertically. The correlation matrix of the model can be easily formulated after knowing the entries in the fundamental matrix.

(d) Sensitivity matrix for the basic model

For 2-D underseepage, no analytical solution such as Eq. 3.1 for 1-D underseepage is available to express h in terms of k. Hence, the derivation of sensitivity matrices for 2-D underseepage study is fully dependent on numerical procedure using the finite element program, FEDAR, described in Chapter II.

Sensitivity matrices obtained for different permeability increments no longer have the desired property of being in constant proportions to one another. Variability coefficient can not be calculated according to its original definition in Chapter III. An alternative definition of variability coefficient is as follows:

$$V.C. = \frac{(\sigma_{h\ max})_p}{(\sigma_{h\ max})_{50}} \tag{4.8}$$

where $(\sigma_{h\ max})_p$ is the maximum of σ_h obtained for the underseepage model if the A matrix is formulated based on p% permeability increment. Eq. 4.8 assumes that $\Delta k = 50\%$ is the reference increment. For the 1-D case, this definition of V.C. is exactly equivalent to the previous definition of V.C. The only difference is that one has to carry out an extra step in calculating σ_h according to Eq. 2.9 before the V.C. can be determined.

For our 2-D model, we can calculate the variability coefficients for different permeability increments according to the definition in Eq. 4.8. Fig. 4.5 shows the variation of the variability coefficients calculated for different permeability increments. It is clear from Fig. 4.5 that for our 2-D model, h is no longer linear in terms of the resistivity. h is also a nonlinear function of k or log k. In Section 3.2(e), we saw that by using the equivalent slope method to correct for the nonlinearity, we can obtain consistent σ_h prediction, regardless of the way the sensitivity matrix is formulated. In this 2-D underseepage study, we have decided to formulate our sensitivity matrix based on linearized functional relationship between h and log k. The same results would have been obtained if linearization was in terms of k or 1/k.

4.2 Results from 2-D Underseepage Study

(a) σ_h of the basic 2-D model

σ_h from FOSM analysis of the basic model is shown in Fig. 4.6. The figure shows that σ_h is symmetrical with respect to the center lines of the underseepage path in both the vertical and horizontal directions. The contour lines of equal σ_h, if plotted, will be almost vertical, indicating that for the basic 2-D model, there is no significant variation of σ_h in the vertical direction. This lack of variation of σ_h in the vertical direction is the result of the chosen long vertical scale of fluctuation (225') as compared to the 100' width of the underseepage section. In Section 3.2(c), we saw that for the 1-D case, when θ becomes very large, all the blocks tend to act as a unit with a single but unknown permeability. In this case, for large θ_y^k, all the blocks in the vertical direction act as a unit, thereby reducing the 2-D model to its 1-D equivalent. In Chapter III, we showed that boundaries are important in reducing seepage uncertainty. When we consider correlation in the vertical direction for our 2-D model, however, we find that even though θ_k^y is much larger than the width of the underseepage section. σ_h does not reduce to zero as in the case for 1-D underseepage. The reason is that the boundary potentials in the vertical direction are not fixed. Therefore, the presence of top and bottom boundaries does not inhibit the growth of σ_h with θ_k^y.

We carry the above discussion further by considering the case when θ_k^y is very large. Table 4.1 compares σ_h for the 2-D model with θ_k^y = 5000 feet and θ_k^x = 225 feet with the values for the basic 1-D model from Chapter III. The two sets of results agree to within 2%. This shows that 2-D analysis is consistent with 1-D analysis, with the latter being a

special case of the more general 2-D analysis. The results also increases our confidence in the use of equivalent slope method to correct for non-linearity in 2-D underseepage study.

(b) Variation of scale of fluctuation in the vertical direction

Head uncertainty, as measured by σ_h, is shown in Fig. 4.7 for θ_k^x = 225 feet and θ_k^y = 10 feet. For this situation, σ_h is only about 40% of the σ_h for the basic model whose θ_k^y is 225 feet. This decrease in σ_h can be explained by the property of water being able to flow around obstacles (as discussed in Section 4.1). The effect of this "flow-around" property is the reduction in seepage uncertainty. Dettinger (1979) observed the same kind of reduction for their 2-D seepage model. However, the slight increase in σ_h at the boundary is not observed here. This is probably due to the different manner by which the seepage path is being discretized. Dettinger discretized the continuous medium into a mesh containing a perpendicular network of flow channels. This type of discretization is necessary for their finite difference methodology. The present study, however, subdivides the medium into rectangular blocks. The question of discretization has been addressed in Section 3.2(b). It was shown that this type of discretization is an adequate representation of a continuous medium.

The effect of θ_k^y on $\sigma_{h\ max}$ is plotted in Fig. 4.8. θ_k^x for all cases remains constant at 225 feet. The plot shows that as θ_k^y decreases, $\sigma_{h\ max}$ approaches zero. This is because $\Gamma^2(V|U)$ in Eq. 4.1 goes to zero as θ_k^y approaches zero. As θ_k^y becomes larger, $\sigma_{h\ max}$ increases monotonically until it reaches the asymptotic limit defined by the 1-D model. Fig. 4.8 also shows that when θ_k^y becomes greater than two times the width of the

underseepage path, a 1-D model can be used to predict the seepage uncertainty with less than 10% error.

(c) Variation of scale of fluctuation in the horizontal direction

The effect of θ_k^x on $\sigma_{h\ max}$ is plotted in Fig. 4.9. θ_k^y is 30 feet for all cases. The effect of θ_k^x on σ_h is identical to that for 1-D underseepage. Head uncertainty, σ_h, is zero when θ_k^x is zero. It peaks when θ_k^x is at about 250 feet and decays back to zero asymptotically when θ_k^x becomes very large.

(d) Output correlation functions

The output correlation functions, ρ_{h_x} and ρ_{h_y}, for the horizontal and vertical directions, respectively, are plotted in Fig. 4.10. The input correlation function for permeability is an isotropic function whose scales of fluctuation in both directions are equal to 30 feet. Scales of fluctuation for output correlation functions are much larger than 30 feet. This is consistent with the observation in Chapter III.

Values of ρ_{h_y} for distances greater than 100 feet are unavailable because our underseepage path is only 100 feet wide. However, judging from the way the correlation functions decay in Fig. 4.10, it is clear that θ_{h_y} will be larger than θ_{h_x}. Despite the fact that the input scale of fluctuation is isotropic, the output scale is not. Bakr et al (1978) also noticed that h is correlated over a larger distance in the direction transverse to the mean flow path than along the flow. The reason for this anisotropy is again due to the non-varying end boundary potentials specified for the model. The high correlation in the vertical direction is an useful information for an engineer who considers placing, say, two piezometers along the same transverse section of a dam. If one of the piezometers

measures a head which deviates by a certain amount from the head predicted by the deterministic flow net, then he can expect with relatively high certainty that the second piezometer will deviate by approximately the same amount (because of the large head correlation in this vertical direction). If the deviations differ substantially from each other, then he should question the accuracy of the assumptions he made in arriving at his deterministic predictions.

(e) Other factors that affect σ_h

By direct analogy with the 1-D study, the following can be said about the behavior of a 2-D model:

First, the model is not sensitive to the degree of discretization. The results obtained above will not be different if the underseepage path is discretized into more elements. The important point is to appropriately correct for the nonlinearity (using the equivalent slope method). A significant portion of the error is actually caused by numerical round-off in the computer program. Following the experience from the 1-D study, discretization is considered to be adequate if the element length is no more than twice the scale of fluctuation. Although rectangular elements were used in the 2-D model, the behavior of the model is actually continuous, and is governed entirely by its scales of fluctuation. Such is not the case with Monte Carlo simulation approach which introduces artificial boundaries between two adjacent elements.

Again, for the 2-D case, the constant σ_h, such as what is obtained analytically, would exist only when θ is a very small fraction of the underseepage length because of the effect of finite boundaries.

For the 2-D model, $\sigma_{\log k}$ is chosen to be 0.25. The methodology could have been applied to higher values of $\sigma_{\log k}$. Since k is assumed to be distributed lognormally, the sensitivity matrix, if formulated based on log k, should be an invariance regardless of the value of σ log k. Head variance, σ_h, will be exactly proportional to σ log k. This is an added advantage of formulating the sensitivity matrix based on linearization of the functional relationship between h and log k.

(f) Realistic dam section

All of the above analysis has been carried out on a 2-D model which assumes that the soils, both upstream and downstream of the dam, are infinitely pervious. The purpose of this idealization is to enable direct comparison between 1-D and 2-D results.

In this section, pore pressure variability in a real dam section will be examined. The boundary condition of infinite permeability will be relaxed resulting in a dam section that is presented in Fig. 4.11(a).

The results from FOSM analysis of the section is included in Fig. 4.11(b). This is compared to σ_h for the idealized model with the same set of statistical parameters in Fig. 4.11(c). Fig. 4.11(b) shows that for real dams, σ_h is not constant in any vertical section, although the variation is less than 1-2% except at locations near the upstream and downstream ends of the dam.

Fig. 4.12 compares the σ_h profile for the idealized 2-D model with those from real dams along different horizontal sections. The σ_h profile for the top flow line agrees within 2% with the idealized model. The reason is that the top flow line for a real dam is basically horizontal. Except for a small portion of the seepage path that is within 50 feet of

the two ends, the 2-D idealized model can also predict with over 90% accuracy σ_h for the bottom flow line. This study shows that the idealized 2-D model gives a good estimate of the seepage uncertainty in real dams.

(g) 3-D extension of 2-D underseepage study

It is possible to extend the 2-D methodology to a 3-D underseepage study. The 3-D model will consist of discretized volumes with m_k, σ_k and θ_k in all three directions. An equation, analogous to Eq. 4.7, can be derived for the covariance between spatial averages over two volumes at a fixed distance apart. The equation will contain 64, rather than 16 terms. A sensitivity matrix for 3-D flow can be derived through a 3-D flow analysis.

The 3-D model differs form the 2-D model in that water is allowed to flow in the third direction. However, if the ability to circumvent obstacles is a valid explanation for the variance reduction going from a 1-D to a 2-D analysis, then σ_h obtained from a 2-D analysis is expected to be very close to σ_h from a 3-D analysis because of the following argument:

First of all, notice that the results from 2-D analysis are equally applicable to a horizontal section through a dam with θ_k^y being replaced by θ_k^z the scale of fluctuation in the z direction. A section with the smallest θ in the direction transverse to the mean flow path will provide the greatest opportunity for flow to circumvent an obstacle. If a 2-D analysis is carried out on the section with minimum θ, the results obtained should not differ much from the result of a 3-D analysis since the behavior of 3-D models will be governed by the section with smallest θ. This discussion is consistent with what Dagan (1979) concluded from his study of seepage uncertainty.

4.3 Discussion of 2-D Underseepage Study

The 2-D model discussed in this chapter is a simple but accurate representation of the underseepage behavior of a dam. It is a logical extension of the 1-D study in Chapter III. Although the study in this chapter has been carried out on an idealized 2-D section, the results and the conclusions from the study would not have varied much had the study been carried out on a real dam section. This is because most of the flow paths underneath a dam are close to being horizontal (Section 4.2(f)).

The study is based on a set of chosen statistical parameters which are quite realistic for dams. Quantification of σ_h is not intended here, but it can be done once the statistical parameters for a particular dam are known. This study of 2-D models shows that much of the variability in seepage uncertainty is caused by the variation of θ_k^x and θ_k^y, besides the variance of the permeability.

Once again, the study is restricted to steady state rather than transient flow through the dam. Anisotropy in material properties, besides that of the correlation function, has not been treated here. It can be done by rescaling the vertical direction and transforming it into an isotropic equivalent. The output correlation function for heads does not have a definite relationship with the input correlation function, except that the output scales of fluctuation are always larger than the input scales because of the averaging process involved.

4.4 Conclusions

The following can be concluded from the 2-D study:

(1) The 2-D underseepage study is consistent with the 1-D study, with the latter being a special case of the 2-D study. The two models are exactly the same if the scale θ_k^y in the 2-D model is equal to infinity.

(2) For the 2-D model, σ_h is zero when $\theta_k^y = 0$. As θ_k^y increases, σ_h increases and converges asymptotically to the σ_h from the 1-D model.

(3) σ_h varies with θ_k^x in exactly the same manner as the 1-D model.

(4) Despite assumed isotropy in the input (permeability) correlation structure, the output (pore pressure) correlation function is anisotropic. Head is correlated over a longer distance in the vertical than horizontal direction. Output scales of fluctuation are both much larger than the input scales of fluctuation.

(5) The behavior of the 2-D model with respect to changes in $\sigma_{\log k}$ and to the number of discretized units is the same as for the 1-D model. Rigorous analytical solutions of σ_h should not be applied to study seepage uncertainty in dams because of the effect of finite boundaries.

(6) σ_h from idealized dam section agree very well with σ_h from real dam.

(7) 2-D analysis on a critical section of a dam will produce approximately the same result as a 3-D analysis, so, a 3-D analysis of underseepage problem is not necessary.

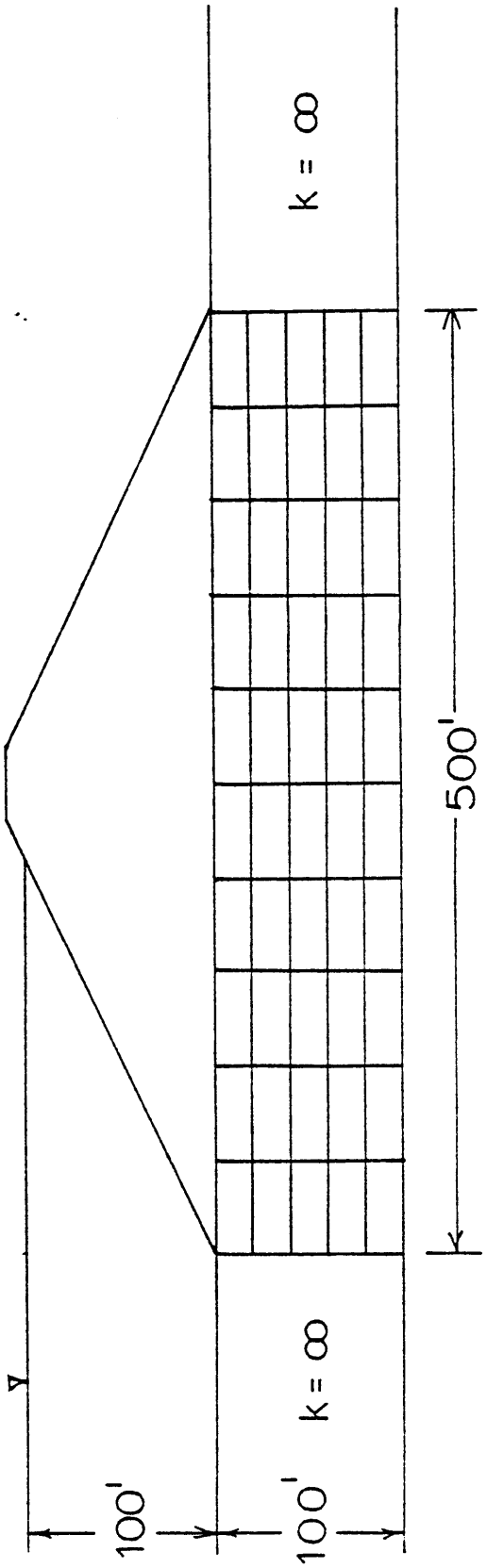

FIG. 4.1 BASIC 2D UNDERSEEPAGE MODEL

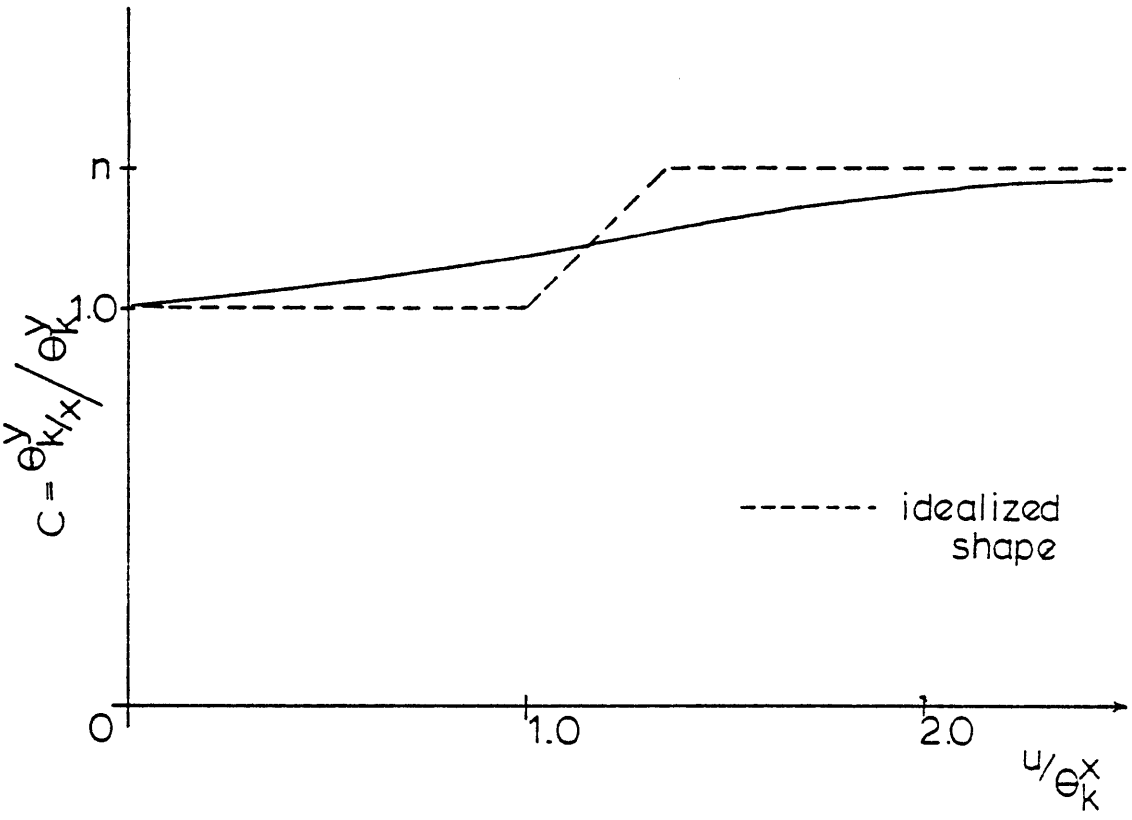

FIG. 4.2 COUPLING BETWEEN θs IN THE x AND y DIRECTIONS

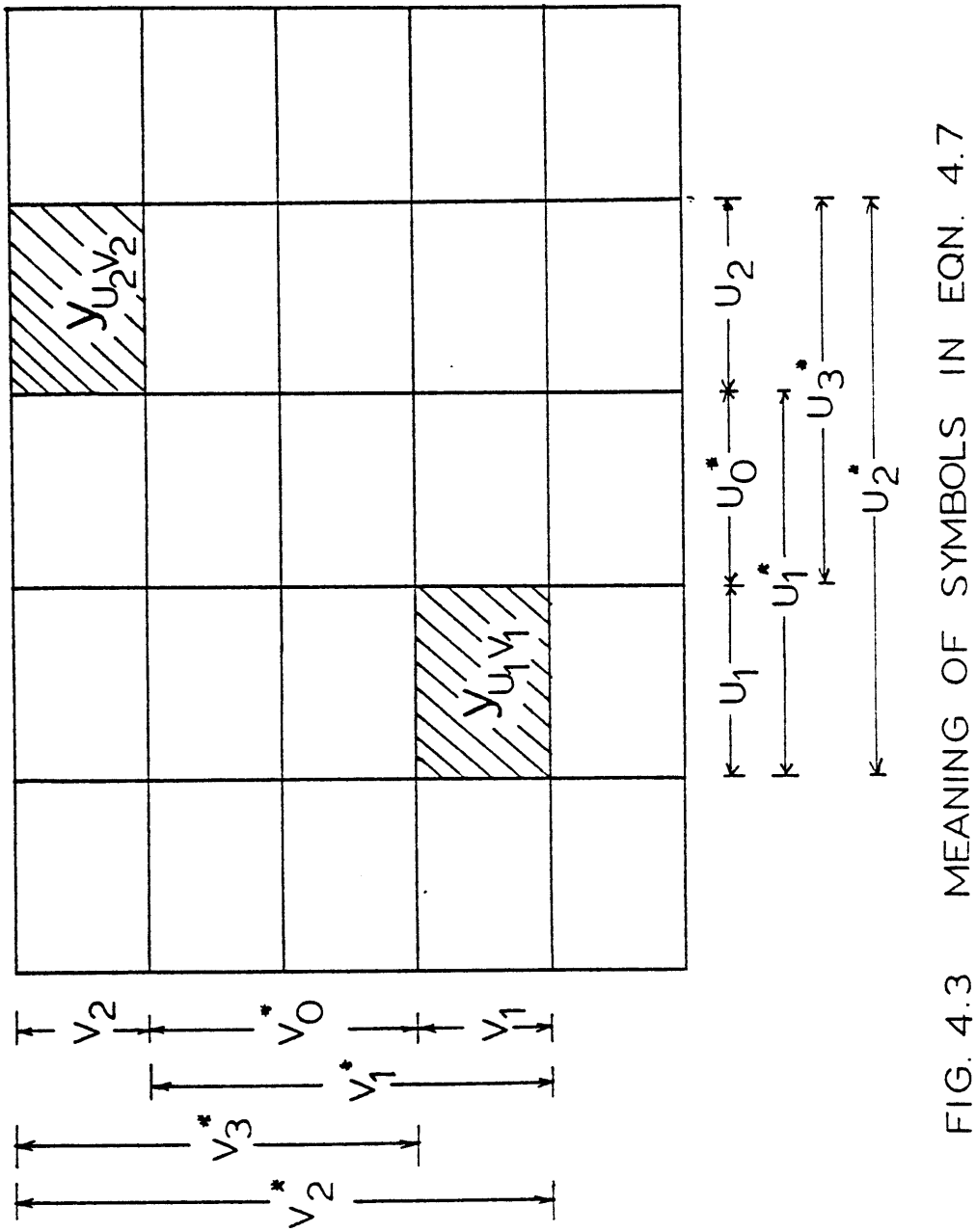

FIG. 4.3 MEANING OF SYMBOLS IN EQN. 4.7

500'

100'

1.000	0.840	0.600	0.360	0.125	0.005	0.000	0.000	0.000	0.000
0.997	0.838	0.598	0.359	0.125	0.005	0.000	0.000	0.000	0.000
0.993	0.834	0.596	0.358	0.124	0.005	0.000	0.000	0.000	0.000
0.989	0.831	0.594	0.356	0.124	0.005	0.000	0.000	0.000	0.000
0.985	0.828	0.591	0.355	0.123	0.005	0.000	0.000	0.000	0.000

FIG. 4.4 Fundamental correlation matrix for the 2-D basic model

($\theta_k^x = \theta_k^y = 225'$)

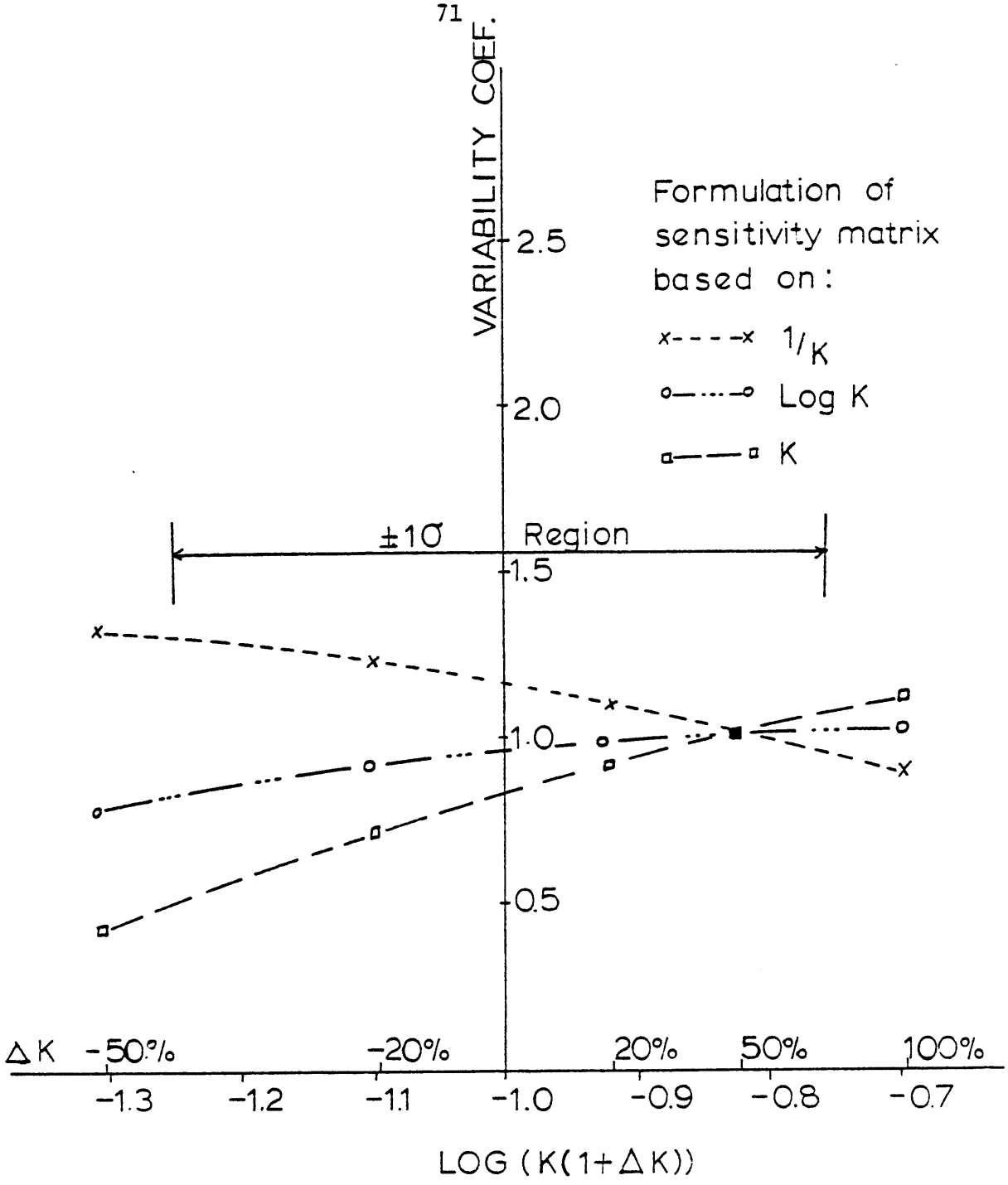

FIG. 4.5 VARIABILITY COEFFICIENTS FOR THE BASIC 2-D MODEL

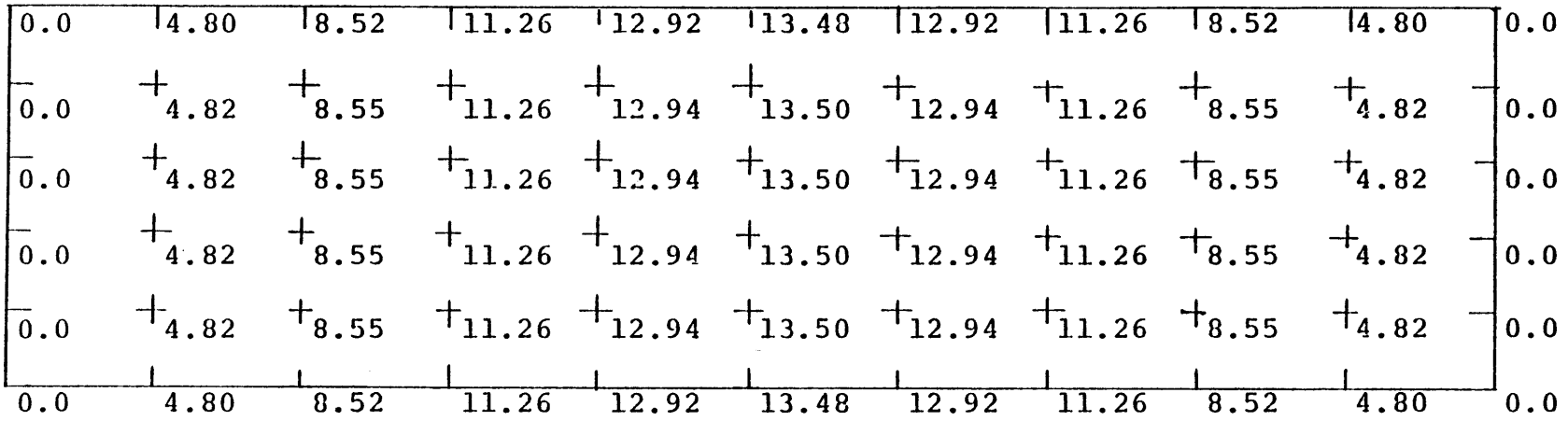

FIG. 4.6 σ_h FOR THE BASIC 2-D MODEL

DISTANCES (FT)	0	50	100	150	200	250
σ_h for 2-D Model $\theta_x^k = 225'$, $\theta_y^k = 5000'$	0.00	5.20	9.22	12.17	13.96	14.57
σ_h for 1-D Model $\theta = 225'$ (fr. TABLE 3.6)	0.00	5.22	9.36	12.38	14.26	14.87

TABLE 4.1 Comparison of σ_h predicted by a 1-D Model with σ_h predicted by a 2-D Model whose θ_y^k is very large

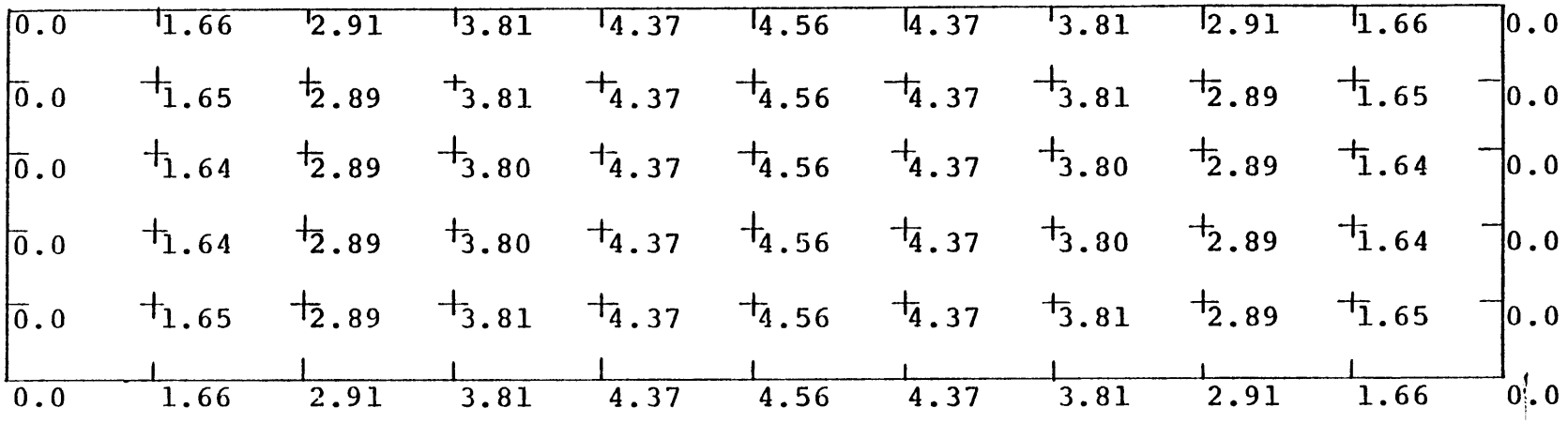

FIG. 4.7 σ_h FOR A 2-D MODEL WITH θ_k^x = 225' AND θ_k^y = 30'

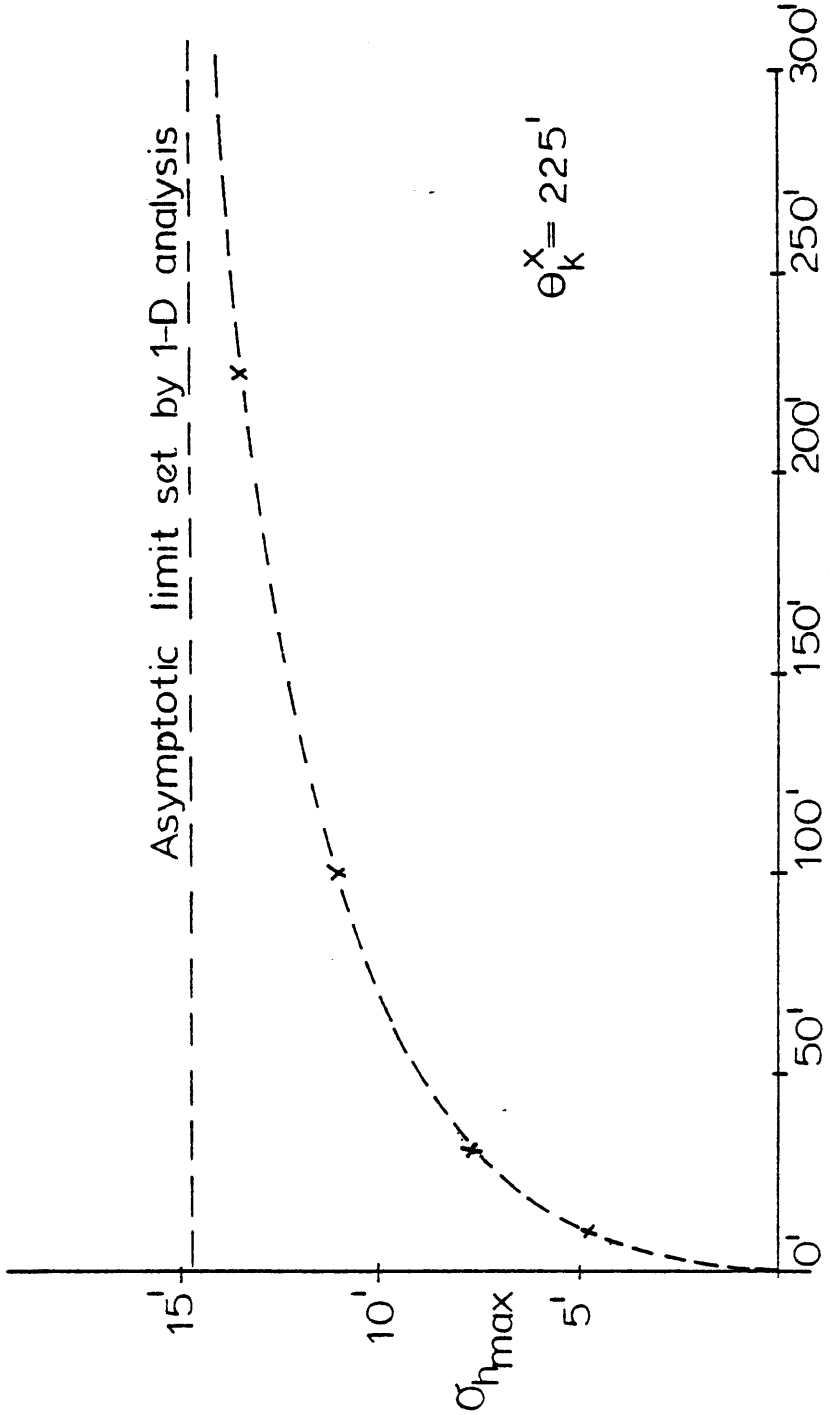

FIG. 4.8 PLOT OF $\sigma_{h_{max}}$ VS. θ_k^y

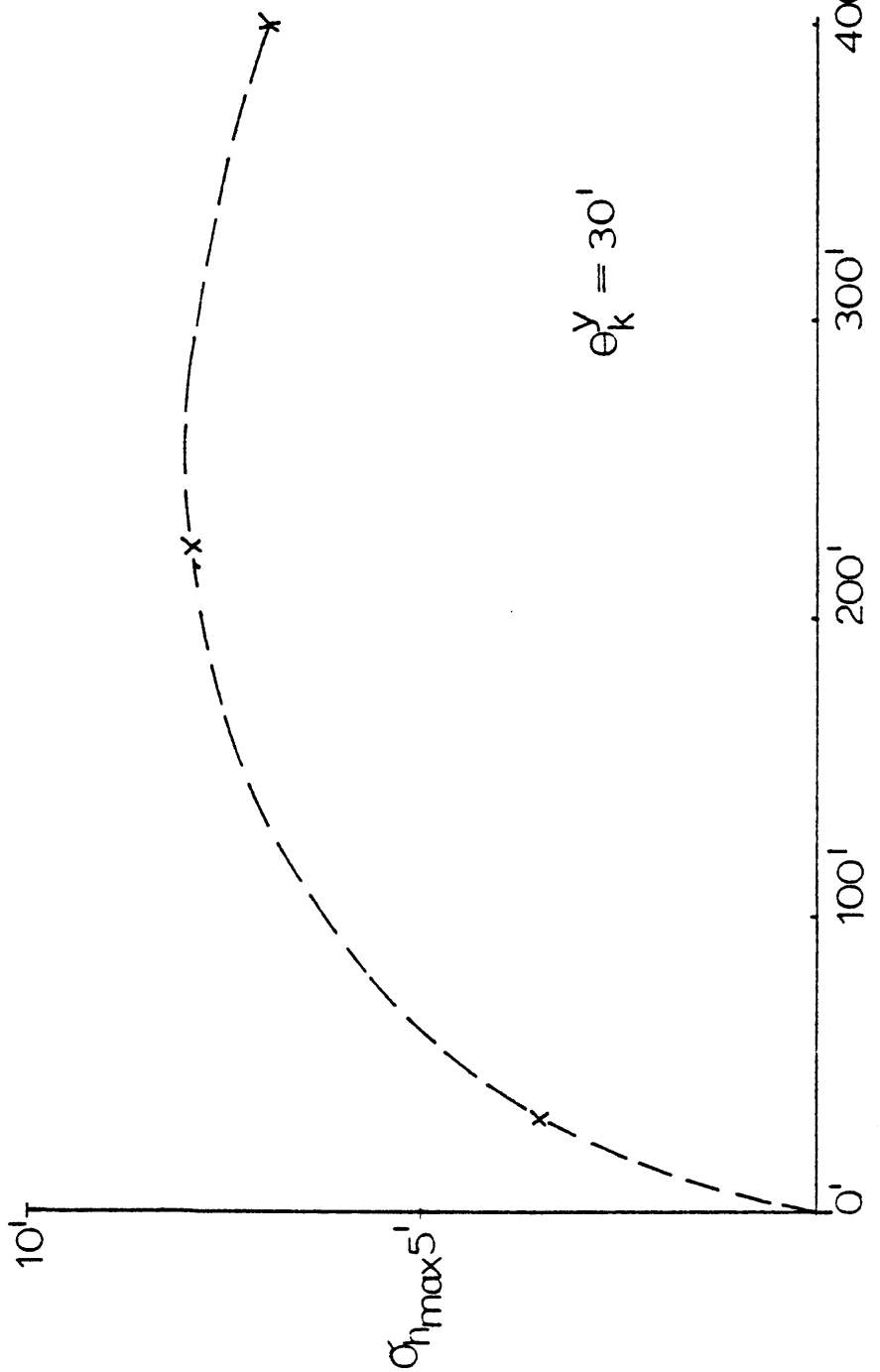

FIG. 4.9 PLOT OF $\sigma_{h_{max}}$ VS. θ_k^x

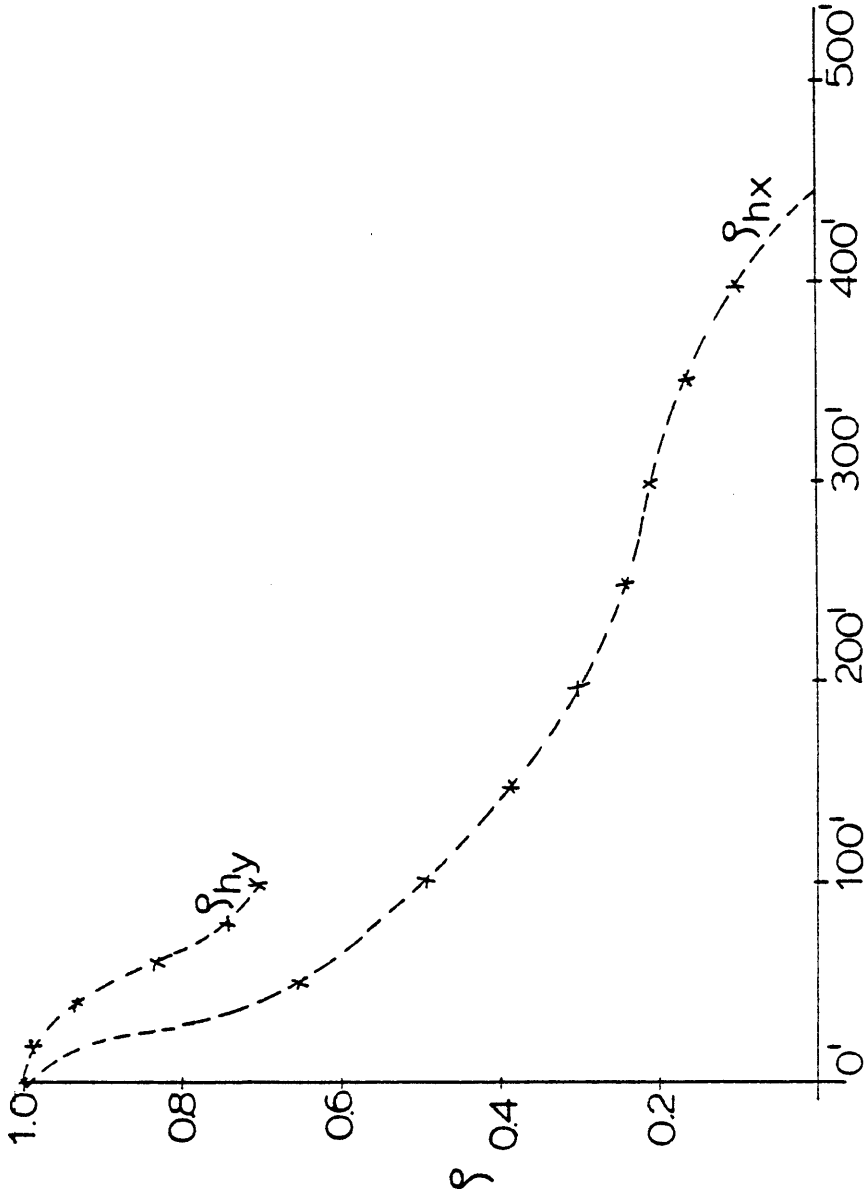

FIG. 4.10 OUTPUT CORRELATION FUNCTIONS FOR $\theta_k^x = \theta_k^y = 30'$

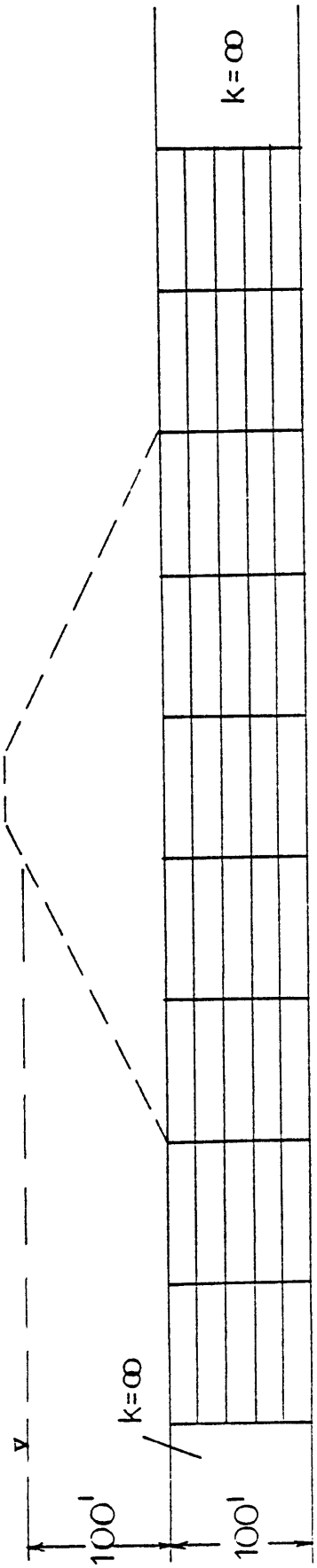

FIG. 4.11(a) A REALISTIC DAM SECTION

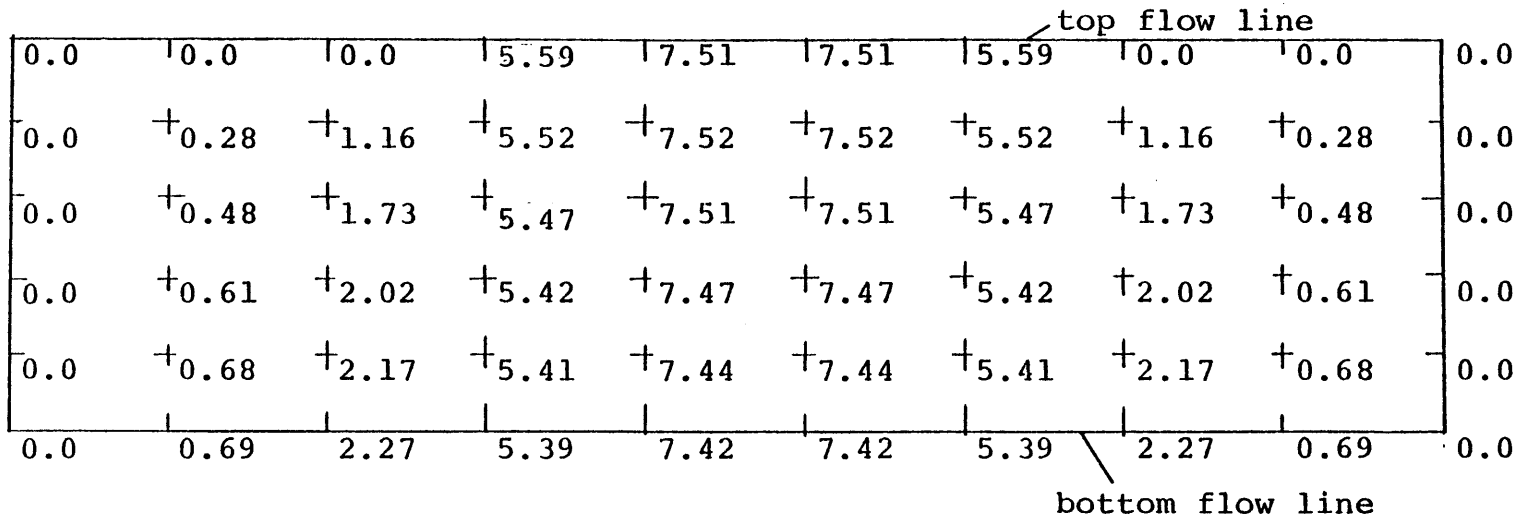

FIG. 4.11(b) σ_h FOR THE REALISTIC DAM SECTION ($\theta_k^x = 225'$, $\theta_k^y = 30'$)

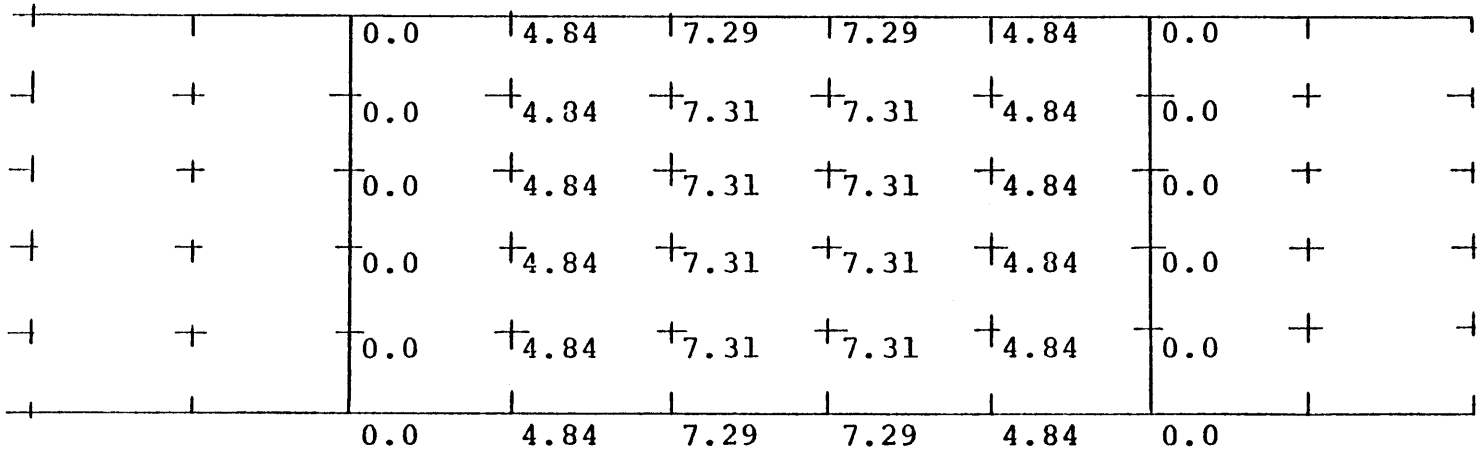

FIG. 4.11(c) σ_h FOR THE IDEALIZED UNDERSEEPAGE SECTION ($\theta_K^X = 225'$, $\theta_k^y = 30'$)

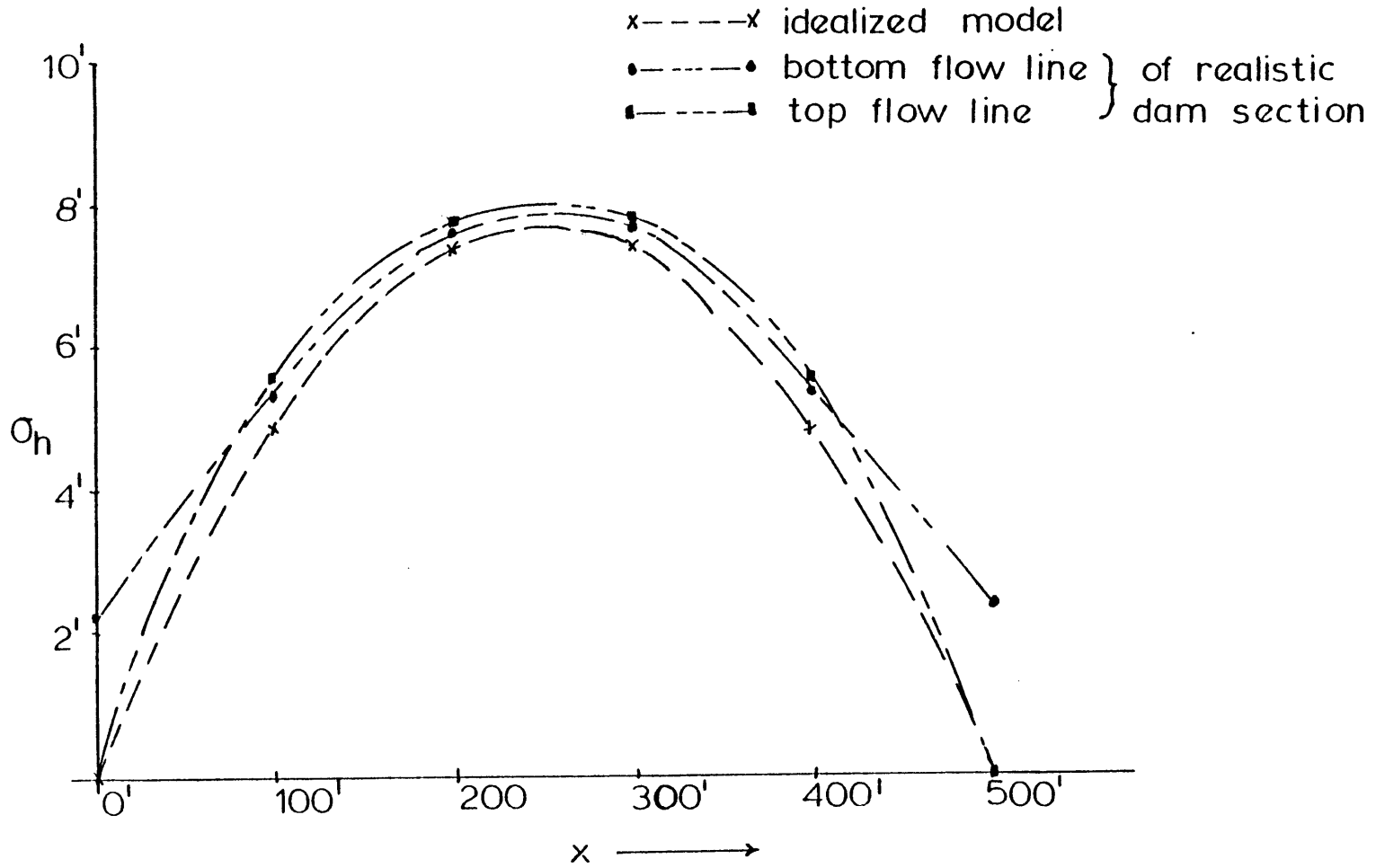

FIG. 4.12 COMPARISON OF σ_h FROM THE IDEALIZED UNDERSEEPAGE SECTION WITH σ_h FROM REALISTIC DAM SECTION

CHAPTER V ANALYSIS OF UNDERSEEPAGE IN DAMS

5.1 Introduction

In the previous chapters, we saw the successful application of FOSM methodology to the study of variability of head in both one and two dimensional underseepage situations. Parametric study of the underseepage models has led to a better understanding of various factors contributing to seepage uncertainty.

In this chapter, the same FOSM methodology will be applied to the analysis of seepage related problems in dams. The major concern of this chapter is restricted to the use of piezometers to monitor underseepage performance of dams. It must be emphasized that there are many other potential applications of the methodology developed. Some of the other applications will also be briefly discussed.

The safe operation of a dam is a direct function of how well its seepage behavior is understood and controlled. The importance of seepage control is reflected by the fact that a large percentage of dam failures is caused by seepage related problems. Table 2 from Middlebrooks' (1953) collection of dam failures from 1914 to 1950 is presented in Fig. 5.1. Seepage related failures account for more than one quater of all the dam failures cited by Middlebrooks. This figure does not include failures by conduit leakage, which are in turn often caused by piping around the conduits (also seepage related). More recent study by ICOLD (1974) also shows that seepage related problems constitute the single most important cause of dam failures, much more important than other causes such as earthquakes, slope instability, uneven settlement, etc... . Seepage related problems are likely to continue their dominance over all other

problems as engineers are forced to build dams on increasingly more difficult and less favorable sites, subjected to the increasingly adverse loading of higher head difference because of the demand for increasing dam heights.

Through years of men's cumulative experience with dams, a set of standard seepage control features have evolved. These seepage control features comprise what is generally regarded as "good engineering design" against seepage induced problems. In this study, these features are broadly classified into two categories; i.e. the active and the passive seepage control measures. Both active and passive seepage control measures will be described in further details later.

Ideally, if all seepage control measures were included at the right locations,within a dam, the hazard of seepage related dam failures would be extremely small. In practice, however, total seepage control can seldom be achieved. Economic constraints always preclude full-fledged subsurface exploration so that a dam is usually designed based on incomplete information about foundation conditions. Failure to conform with design specifications and construction difficulties are important issues that often lead to much reduced effectiveness of seepage control features.

Because of all the uncertainties, engineers must rely on proper instrumentations to detect conditions which are different from those assumed during the design phase. This is in essence Peck's (1969) observational approach.

Successful application of the observational approach relies heavily on proper interpretation of instrument readings. In some cases, the discrepancies between measured and expected readings are substantial, making it very difficult, even for a well experienced engineer to explain the

causes of discrepancies. Take the case of pore pressure measurements in a dam, for example. The deviation between actual and predicted pore pressures can be very large (greater than 10 ft. in the case study cited by Marr and Lambe (1979)). According to the investigation by Mathew (1980), in cases where measured and predicted values do not agree, most engineers use the measured values to backfigure the "correct" parameters to use for their predictions so that the values agree. We learned from the previous chapters that some of the deviations might be within the tolerance of inherent variability. Without properly accounting for this background inherent variability, the engineers have no basis for setting up accurate analysis which can forewarn them of potential problems with the dams.

Section 5.2 in this chapter will describe common seepage related problems in dams. In the following section, we will discuss active and passive seepage control measures normally considered for the purpose of minimizing seepage problems. Section 5.4 will introduce hypothesis testing, a useful statistical procedure suitable for the study in Section 5.5, which will deal with the use of piezometers to monitor the performance of active seepage control measures in the foundation of a dam. Finally, Section 5.6 will give a brief description of other applications using the same procedure as Section 5.5. Section 5.6 will also summarize the results from the study in this chapter.

5.2 Seepage Related Problems in Dams

There are three common seepage related problems in dams. They are described below:

(a) Piping and internal erosion

Piping and internal erosion are usually associated with the gradual washing out of material from either the foundation or the embankment of of an earth dam. Piping is normally related to the progressive formation of channels or "pipes" which usually initiate at the exposed downstream end of a dam. Internal erosion, on the other hand, can occur anywhere within the dam embankment or foundation. It usually starts at the discontinuities, such as the interface between two different materials, or at the location of a crack, perhaps earthquake-induced. Both piping and internal erosion, if left progressing and unchecked, will eventually lead to the collapse of the dam.

The mechanisms that lead to piping and internal erosion are still not very well understood. High seepage gradient is necessary but the criteria for critical gradient cannot be established except for the case of an upward flow in cohesionless material. Under laboratory conditions, some clays can resist piping even under hydraulic gradients which are in excess of 1000 (Kassif et al (1965)). Piping and internal erosion can also be caused by the migration of fine particles from an unprotected fill into neighboring zones consisting of much more pervious materials, whose pore sizes are larger than most of the particle sizes of the unprotected fill. That is why many dam failures are initiated by the washing out of fine particles into the drain or the zone of uncompacted material around the concrete appurtenant structures. Piping and internal erosion may also be initiated in cracks caused by an earthquake, uneven settlement, tree roots, animal burrows, etc. . Finally, there are materials which are naturally unstable such as the highly dispersive clay (Sherard (1972)) or soluble limestone in the foundation.

(b) High pore pressure

High pore pressure causes reduction in the effective stress in the soil, which is directly related to the soil strength and to the ability of the soil to support loads. Therefore, the stability of dam decreases with increasing pore pressure. High pore pressure can also cause extensive downstream heaving which is the initiating event for foundation instability.

There are many causes of high pore pressure. Most of them are related to unanticipated foundation conditions. The most common cause of high downstream pore pressure is a shortening of the underseepage path. Shortening of the underseepage path can be caused by a crack at the foundation embankment interface due to differential settlement, or by the presence of very pervious foundation anomalies at the upstream end of a dam. A relatively impervious blanket at the downstream end of the dam can also lead to high downstream pore pressure. Upstream slope failures are usually attributed to the slow dissipation of excess pore pressure compared to the rate of drawdown. Cyclic shearing of soil due to earthquake can also induce high pore pressure, the extreme effect of which is a flow slide following extensive liquefaction.

(c) Excessive loss of water

Excessive loss of water is only important from the functional or serviceability viewpoint (rather than from structural safety viewpoint). It can be an important concern for dams in arid regions, where water is a valuable commodity. It is also an important concern for power generating dams which cannot maintain constant head difference because of excessive seepage losses.

5.3 Seepage Control Measures in Dams

Common seepage control measures in dams can be broadly classified into active and passive controls. A control feature is called active if it actually interferes with the seepage, producing a more desirable seepage condition. Passive controls do not interfere with the seepage. However, they help to produce an environment less susceptible to seepage induced problems.

(a) Active seepage control measures

There are many types of active seepage control measures in dams. The five most common measures are: drainage, grouting, impervious cutoff, upstream impervious blanket and relief well.

Drains have become standard features in modern dams. It is much easier to predict the seepage pattern with the presence of a drain. We know that any seepage through the dam will be diverted through the drain because of its high permeability compared to the surrounding materials. The most common type of drain is the downstream horizontal drain. A downstream horizontal drain is usually supplemented by a vertical intercepter drain which is useful in collecting seepage through horizontal pervious layers that might have bypassed the horizontal drain and rendered it useless. The pervious layer might be a horizontal layer of uncompacted material in the embankment, or an undetected layer of very pervious material in the foundation such as a buried old river channel. A drain will only work well if it is unclogged. Clogging decreases the permeability of the drain, thus, reducing its ability to divert seepage. Clogging is usually caused by the washing-out of particles into the drain if it is not protected by an adequate layer of filter. The washing-out of particles

can also lead to piping and internal erosion of the material surrounding the drain.

Foundation grouting helps to reduce the amount of seepage. It is also useful in reducing downstream pore pressure. Grouting, however, creates a localized region of high pore pressure and seepage gradient. Therefore, grouting is always found in the upstream end of the foundation where high pore pressure and high seepage gradient have a lesser influence on the overall stability of a dam. The purpose of grouting is to reduce the permeability of the grouted zone. In practice, it is very hard to determine the magnitude of reduction. It is a function of many factors such as grouting pressure, grout mix, foundation permeability, foundation characteristics, grout hole spacing, etc. .

An impervious cutoff works the same way as a grouted zone; the latter is actually a special case of impervious cutoff. There are many forms of impervious cutoff. Very often, a partial cutoff is formed by extending the impervious core of a dam into its foundation. A cutoff can also be formed by driving a sheet pile wall into the foundation in situations where foundation difficulties preclude the excavation of a cutoff trench. The cutoff characteristic of a sheet pile wall is not well understood and is highly dependent on the construction procedure.

When there are plenty of impervious materials on site, a layer serving as an upstream impervious blanket can be a viable alternative for, or a supplement to, an impervious cutoff of foundation grouting.

A relief well is a good remedial measure against high downstream pore pressure. It punctures the downstream foundation to relieve the high pore pressure. Relief wells have the negative effect of increasing

the quantity of flow and the hydraulic gradient in the foundation due to the shortening of underseepage path.

(b) Passive seepage control measures

Passive controls are as important as active controls in protecting dams against seepage related failure. Examples of passive controls are filters, transitions between zones, good compaction, and careful construction.

Because of the vast difference between the grain size characteristics of a drain and its surrounding materials, filters are usually required to act as transitional materials. A filter must be designed such that it permits free escape of seepage water while retaining the soil particles firmly in place. It can either be single layered or graded. The most commonly used filter criteria are those suggested by Terzaghi (1922):

$$\frac{D_{15}\ \text{(of filter)}}{D_{85}\ \text{(of soil)}} < 4 \text{ or } 5$$

$$\frac{D_{15}\ \text{(of filter)}}{D_{15}\ \text{(of soil)}} > 4 \text{ or } 5 \qquad (5.1)$$

Eq. 5.1 is based on the comparison of the grain size characteristics of the filter material with those of the base material which is to be protected. D_{15} refers to a point on the gradation curve of the soil: 15% by weight of the soil is finer than the D_{15} grain size. Bertram (1940) has shown that this criteria is conservative. Subsequent modification to the criteria has been proposed by the Corps of Engineers (1941)

and by Karpoff of the Bureau of Reclamation (1955). Silveria (1965) derived theoretically the thickness of filter required to prevent full penetration of fines from the base material. Cedergren (1960) determined from flow net analysis the thickness of filter required to permit free passage of seepage water.

A transition, as its name implies, is that layer of soil which acts as a transition to prevent materials with different gradations (and other characteristics) to come into direct contact with one another. The behavior (strength, compressibility, permeability) of the soil that functions as a transition is intermediate between the two materials being protected. For example, a transition helps to reduce the probability of crack formation at the interface of two materials which have vastly different settlement characteristics. Transitions are important design features at locations such as foundation-embankment interface, around concrete appurtenant structures, etc. .

Careful construction is also a passive measure against the development of seepage related problems. Segregation of filters and transitions during construction can drastically reduce their effectiveness. One of the important causes of dam failures cited by Middlebrooks (1953) is piping around conduits, caused by inadequate compaction of the soils around the conduits.

Finally, a general category called "good design" fits well into the discussion of passive measures. Intelligent choice of materials for the dam can prevent potential seepage problems. The decision to avoid using broadly graded materials such as glacial till is an example. Piping and internal erosion problems often occur in glacial till. Careful zoning can also achieve reduced hazard against seepage induced problems. More

effort should be devoted to the study of the effects of different geometrical configurations of dams. As an example, we cite the study by DeMello (1977) on the most effective inclination of a chimney drain in a dam.

5.4 Hypothesis Testing

Let us suppose that an engineer had designed an active seepage control feature that has the net effect of changing the expected piezometric head at location z from h_{1z} down to h_{0z}. If he observed a piezometric head h_z which is different from the predicted value, h_{0z}, can he, by any rational procedure, deduce whether his design is working properly and with what level of confidence can he say that his deduction is accurate?

A convenient and powerful statistical procedure called hypothesis testing will allow us to answer the above question. We can set up two hypotheses about the "state of nature" of the dam as follows:

H_0: normal condition : active control feature works as planned

H_1: adverse condition: ineffective control

H_0 is known as the null hypothesis. For the cases to be considered in Section 5.5, H_0 is the condition which the engineer hopes to achieve. On the contrary, H_1 is the alternate hypothesis which defines the undesirable state of the dam.

In the previous chapters, we have developed a practical procedure for obtaining information about variablity in piezometric heads. We can use the same procedure to obtain the variability of heads under the null and the alternate hypothesis. Given the actual measured head, hypothesis testing permits us to identify the relative likelihood that either H_0 or H_1 is true, and the associated confidence we have in our deduction.

Hypothesis testing will only be briefly described here. Readers are referred to standard textbooks on statistics, e.g., Benjamin and Cornell (1970), for further information.

For simplicity, we will only consider a one-sided, discrete two-state type of hypothesis testing. Let the distribution of head at point z under the null hypothesis be represented by the probability density function shown in Fig. 5.2(a). The mean and standard deviation of the distribution are $m_{h_{0z}}$ and $\sigma_{h_{0z}}$ respectively. Although the expected h at z is $m_{h_{0z}}$, a piezometer installed at location z can indicate virtually any reading because of the spread of the probability density function. The probability of reading a value somewhere between h_1 and h_2 ($P(h_1 < h_{0z} < h_2)$) is simply the area under the probability density function between h_1 and h_2, as shown in the figure. The probability of h_{0z} being smaller than h_{crit} is $1-\alpha$. α is defined as the level of significance. It is the shaded area under the probability density function greater than h_{crit}. The cumulative distribution function is shown in Fig. 5.2(b). It is the plot of $1-\alpha$ against h_{0z}.

In hypothesis testing, we choose the level of significance we want, typically 0.01, 0.05, or 0.10. Knowing α, we can then determine h_{crit} for any given distribution of h. If h_z, the measured piezometric head at z, is greater than h_{crit}, we can reject the null hypothesis at α level of significance. We cannot reject h_0 if h_z is less than h_{crit}. α is also defined as the type I error of the test which is the probability of rejecting H_0 given that H_0 holds.

Notice that just because we cannot reject H_0 does not mean that we have to accept H_0. The reason is that h_z could also have been generated by the probability density function of the alternate hypothesis, H_1.

Type II error of the test, β, is by definition the probability of not rejecting H_0 given that H_1 is true (i.e., $P(h_{1z} < h_{crit})$). The power of the test is simply equal to $1-\beta$. Fig. 5.3 will illustrate the two contrasting cases for hypothesis testing. In Fig. 5.3(a), $m_{h_{0z}}$ and $m_{h_{1z}}$ are very close together, therefore the power of test is very low and is approximately equal to α if $\sigma_{h_{0z}}$ is equal to $\sigma_{h_{1z}}$. On the contrary, we have a very powerful test for the situation depicted in Fig. 5.3(b) when $m_{h_{0z}}$ and $m_{h_{1z}}$ are far apart. The power of test for Fig. 5.3(b) is very close to 1.0. Naturally, we would prefer to be in the situation shown in Fig. 5.3(b) where we have high discriminating power between the two hypotheses. The meaning of α and β is summarized in the 2 x 2 matrix shown in Fig. 5.4.

In this study, h will be assumed to be normally distributed. We have to choose a distribution for h because the FOSM analysis does not provide us with any information about higher moments for the probability distribution of h. For any given level of significance, α, we can express h_{crit} as:

$$\Phi\left(\frac{h_{crit} - m_{h_{0z}}}{\sigma_{h_{0z}}}\right) = 1-\alpha$$

$$\frac{h_{crit} - m_{h_{0z}}}{\sigma_{h_{0z}}} = \zeta_{1-\alpha}$$

or

$$h_{crit} = \zeta_{1-\alpha}\, \sigma_{h_{0z}} + m_{h_{0z}} \qquad (5.2)$$

In Equation 5.2, ζ is the standardized normal variable whose mean and standard deviation are 0 and 1 respectively. Φ is the cumulative distribution function of ζ. Values of the standardized normal distribution are tabulated in most statistics books.

The power of test, $1-\beta$, is:

$$
\begin{aligned}
1-\beta &= 1 - P(h_{1z} < h_{crit}) \\
&= 1 - \Phi\left(\frac{h_{crit} - m_{h_{1z}}}{\sigma_{h_{1z}}}\right) \\
&= 1 - \Phi\left(\frac{\zeta_{1-\alpha}\,\sigma_{h_{0z}} + m_{h_{0z}} - m_{h_{1z}}}{\sigma_{h_{1z}}}\right) \\
&= 1 - \Phi\left(\frac{\zeta_{1-\alpha} - \dfrac{m_{h_{1z}} - m_{h_{0z}}}{\sigma_{h_{0z}}}}{\dfrac{\sigma_{h_{1z}}}{\sigma_{h_{0z}}}}\right)
\end{aligned}
\tag{5.3}
$$

Equation 5.3 shows that the power of test for a given α is a function of $m_{h_{1z}} - m_{h_{0z}} / \sigma_{h_{0z}}$, the number of standard deviaitons $m_{h_{1z}}$ is away from $m_{h_{0z}}$; and $\sigma_{h_{1z}} / \sigma_{h_{0z}}$, the ratio of the two standard deviations. Eq. 5.3 is plotted in Fig. 5.5 for α=0.05. Notice that all the curves cross one another at $m_{h_{1z}} - m_{h_{0z}} / \sigma_{h_{0z}} = \zeta_{1-\alpha} = 1.64$. The power of test at the crossing point is 0.5.

By calculating the power of test according to Eq. 5.3, we have a convenient basis for comparing our ability to evaluate the state of nature of the dam using piezometer readings for different cases to be considered in Section 5.5. The statistical parameters, $m_{h_{0z}}$, $m_{h_{1z}}$, $\sigma_{h_{0z}}$, and $\sigma_{h_{1z}}$ can be obtained from FOSM analysis of our H_0 and H_1 model.

Implicit in the above derivation is that there are only two discrete states, i.e., H_0 and H_1. It can be shown that the above derivation is equally valid when $m_{h_{0z}}$ is treated as the maximum mean of h produced by the null hypothesis and α becomes the maximum level of significance of the test. For cases where $m_{h_{0z}}$ is larger than $m_{h_{1z}}$, Eq. 5.4 should be rewritten as:

$$1-\beta = \Phi\left(\frac{\zeta\alpha - \frac{m_{h_{1z}} - m_{h_{0z}}}{\sigma_{h_{oz}}}}{\frac{\sigma_{h_{1z}}}{\sigma_{h_{0z}}}}\right) \tag{5.4}$$

5.5 Use of Piezometers to Monitor the Performance of Active Seepage Control Measures in Dams

(a) Grouting model

Fig. 5.6 shows a grouting model which is set up to study the use of piezometers in monitoring the performance of foundation grouting. The permeability of the grouted zone is assumed to be 1/10 of the permeability of the foundation. Foundation grouting cannot be considered successful unless it meets this ten-fold reduction in permeability. The grouted zone

is assumed to be 50 feet wide as shown in the figure. Two cases are studied, each corresponding to a different location of the grouted zone.

We can set up two hypotheses about the condition of the grouted zone:

H_0: Null hypothesis: $K_{\text{grouted zone}} \leq \frac{1}{10} K_{\text{foundation}}$

H_1: Alternate hypothesis: $K_{\text{grouted zone}} = K_{\text{foundation}}$

(i.e., ineffective grouting)

Table 5.1 summarizes the results from the study of the grouting model. The table presents m_h and σ_h at the designated nodal points for the alternate hypothesis and for the null hypothesis with two different locations of the grouted zone. The power of test at each of the nodal points for $\alpha = 0.05$ was also calculated according to Eqs. 5.3 and 5.4. Each of the nodal points considered is representative of the vertical section through the point because σ_h varies by less than 1% in the vertical direction under both the null and the alternate hypotheses. m_h is constant in the vertical direction.

For any given location in the foundation, we can calculate the h_{crit} corresponding to a particular level of significance, α, and the values of $m_{h_{0z}}$ and $\sigma_{h_{0z}}$ at that location. Given the actual field measurement, we can then choose to reject or not reject the null hypothesis based on h_{crit} as explained in the example below.

For case 1 at location D, $m_{h_{0z}}$ and $\sigma_{h_{0z}}$ are 31.6' and 7.55' respectively. At $\alpha = 0.05$,

$$h_{crit} = \zeta_{1-\alpha}\, \sigma_{h_{0z}} + m_{h_{0z}}$$

$$= 1.645(7.55) + 31.6 = 44.0'$$

At D, a measured head of 40' would pass our test at 5% level of significance because it is less than the h_{crit} calculated. Therefore, we cannot reject H_0 if the measured head is 40'.

The power of test is an index that tells us how well we can assess the performance of grouting using piezometers. Table 5.1 shows that if a piezometer is placed directly downstream of the grouted zone, it has the highest discriminating power between the null and the alternate hypotheses (power of 1.000 and 0.992 for case 1 and case 2 respectively). Perhaps a bit less obvious is the fact that for case 1, a piezometer placed at 250' downstream of the grouted zone has approximately the same power as a piezometer placed directly upstream of the grouted zone (power of 0.851 versus 0.855 for the latter). The power of test for the grouting model at all locations can be considered to be quite good. The overall power of the test for case 1 is slightly better than that for case 2. The power of test for case 1 at D is 0.984. Our decision of not rejecting H_0 when measured head at D is 40' will involve little type II error.

Some of the inferences from Table 5.1 may appear to be too obvious. The reason for that is that a relatively simple grouting model has been chosen on purpose. The intent of this study is to bring out, more in a qualitative than in a quantitative sense, the potential of the methodology for contributing to a greater in depth understanding of the behavior of dams. The results obtained are valuable aids in engineering decision. They help an engineer to

(i) interpret piezometer readings in a rational and consistent manner,

(ii) assess his ability to predict the true state of the dam using piezometer readings, and

iii) plan piezometer locations so as to extract the most amount of pertinent information.

(b) Partial cutoff model

Fig. 5.7 shows a partial cutoff model which will be studied in the similar manner as the grouting model. The cutoff is formed by excavating into the foundation a trench which is backfilled with impervious material and compacted. It is shown as an extension of the impervious core of the dam in Fig. 5.7. Because of the controlled placement of the impervious material, it is possible that the permeability of the cutoff can be as much as 100 times smaller than the surrounding foundation materials.

Therefore, we can set up the following two hypotheses:

H_0: null hypothesis: $K_{\text{partial cutoff}} \leq \frac{1}{100} K_{\text{foundation}}$

H_1: alternate hypothesis: $K_{\text{partial cutoff}} = K_{\text{foundation}}$

(i.e., ineffective cutoff)

The results of the study on partial cutoff are summarized in Table 5.2. In the vicinity of the partial cutoff, σ_h and m_h are not constant in the vertical direction. Two nodal points on the same vertical section are chosen for the region near the cutoff (for example, A1 and A2).

Table 5.2 shows that $\sigma_{h_{0z}}$ for the majority of the nodes are higher than $\sigma_{h_{0z}}$ for the corresponding nodes in the grouting model. The reason is that partial cutoff disturbs the flow a lot more than grouting. The mean flow path for the partial cutoff model is no longer one-dimensional. The overall power of test for the partial cutoff model is quite low (the power is usually below 0.5). This low discriminating power is in part due to the reduced effectiveness of partial impervious cutoff in decreasing

downstream pore pressure, as compared to the fully penetrating grouting cutoff. Higher values of $\bar{\sigma}_{h_{0z}}$ also contribute to the reduction in power. In fact, Table 5.2 tells us that there are only two locations, around nodes A1 and B1, where one can rely on a piezometer to indicate whether the cutoff is as impervious as it was designed to be. The values of the power at nodes A1 and B1 are 0.958 and 0.910 respectively.

(c) Relief well model

Shown in Fig. 5.8 is a relief well model. The results from the analysis on the relief well model is tabulated in Table 5.3. The null hypothesis, H_0, and the alternate hypothesis, H_1, correpond to the cases with and without the relief well respectively.

H_0: relief well works

H_1: relief well does not work

Table 5.3 shows that for all the nodal points, the power of test is very low. The result is not surprising because we know that a relief well is a redundant control in this case. The downstream pore pressure relieved by the relief well is very small. In fact, the use of relief well should not be classified as an active seepage control measure in this case since the seepage pattern is barely altered. Relief well should only be treated as a contingent measure against high downstream pore pressure.

For the same reason, the approach in this chapter is restricted to the study of active seepage control features. Passive controls such as filters and transitions do not change the seepage pattern appreciable enough to be monitored by a piezometer.

(d) Drain model

Fig. 5.9 is the model of a dam with a downstream horizontal drain to control foundation seepage. The seepage model is an idealized 120 feet by 900 feet rectangle with 54 rectangular elements and appropriate boundary conditions. The choice of rectangular elements is necessary because Eq. 4.7 can only handle the correlation between spatial averages over rectangular areas.

The results summarized in Table 5.4 show that piezometers placed directly beneath the drain have high power to discriminate between the null and alternate hypotheses. Much of this power is lost when we move upstream by as little as 200 feet to node C (where the power is only 0.556).

As an aside, notice that the power at nodes G and H are quite high (0.992 and 0.873 respectively). This high power is misleading because the nodal heads is small in either case. The high power arises because of the assumption that instrument error is negligible. Had instrument error been included as an added variance, the power at G and H will be reduced to very small values.

(e) Impervious blanket model

The impervious blanket model is shown in Fig. 5.10. The results from the study of the model is tabulated in Table 5.5.

Table 5.5 shows that the effective location for piezometers is right underneath the impervious blanket, where the power of test is 1.000. A piezometer placed at more than 200 feet downstream of the blanket, because of its low power of discrimination, will not be effective in providing information about the impervious blanket.

5.6 Discussion

In Section 5.5, we saw the successful application of hypothesis testing to the study of the use of piezometers in monitoring the performance of active seepage control features in dams. In a similar fashion, piezometers can also be used to give useful information about the state of a dam with respect to other potential problems. Once again, the first step is to define the hypotheses, H_0 and H_1. H_0, the null hypothesis, may correspond to the adverse condition which we suspect the field piezometer might indicate. H_1, the alternate hypothesis, then corresponds to the state: "suspicion is incorrect," i.e., the dam behaves as designed. FOSM analysis will furnish the required statistical information to carry out hypothesis testing according to the procedure outlined in Section 5.4. The procedure allows us to find out whether the piezometer reading allows us to reject the null hypothesis.

Two examples of some of the problems that can be studied are listed below. These problems are related to foundation seepage. They are the null hypotheses of our tests.

(i) Presence of a crack at the foundation-embankment interface due to excessive differential settlement.

(ii) Existence of undetected foundation anomalies such as zones of very pervious materials, layerings, cavities that can drastically alter the seepage pattern.

The method of hypothesis testing provides a rational basis for determining

(i) whether or not to reject a preconceived notion about what went wrong with a dam, based on piezometer readings

(ii) how well the problem can be diagnosed using piezometers, and

(iii) the optimal piezometer location so as to obtain the maximum amount of useful information.

The method is not restricted only to the study of piezometer readings. Since we know that Q, the quantity of flow, can also be expressed as a function of the permeability, the same procedure can be used to obtain information about the variability of the quantity of flow due to the inherent variability of permeability. The actual quantity of flow can be measured in the field by wiers. We have already developed a procedure for the rational interpretation of field measurements from which logical deductions can be made about the prevailing condition of a dam. The information about quantity of flow can be combined with the information from piezometer readings to form an effective and perhaps inexpensive information package useful for monitoring the seepage performance of a dam.

Thought has also been given to the possibility of extending the approach to the study of piping and internal erosion problems. The obvious difficulty is to determine the criteria for the initiation of the washing-out of particles. The variability of hydraulic gradient can be predicted in terms of the variability of permeability by expressing the hydraulic gradient as a function of the permeability. By using statistics of extremes, we can calculate the maximum hydraulic gradient that the soil will be subjected to and compare it with the critical gradient for washing-out of particles. Because piping and internal erosion are very localized phenomena, we have to look at a much smaller region than before, as shown in Fig. 5.11. The scale of fluctuation should also be a scale which is consistent with the size of the region being studied.

It is believed that this study is a right step towards eventual quantification of the risk of seepage induced failures in dams. It can act as an input to many of the reliability based analyses of dam safety such as the one proposed by Hachich (1980). This study only deals with the interpretation of a single piezometer at one point in time. Hachich will study collective interpretation based on more than one piezometers, the evolution of pore pressure with time, and updating of failure risks based on piezometers readings.

Under normal operating conditions when there are no special problems, the discrepancy between measured and predicted head can be attributed to the inherent variability. The inherent variability of piezometric head is caused by the spatial variability of permeability which can be described by its statistical parameters. It has been assumed that instrument error is negligible. Instrument error can be treated as an added component of variance. Statistical parameters of permeability have the potential of becoming the basis for unifying experiences with discrepancies between measured and predicted heads at different dams. These experiences, until now, have been treated as isolated facts. As mentioned in Chapter II, the statistical parameters of permeability can be derived from analysis of regularly spaced samples. Under control situations, the inverse of the problem can also be done, i.e., deriving the statistical parameters of permeability from the inherent variability of piezometer readings.

	CAUSES OF PARTIAL OR COMPLETE FAILURES	% OF TOTAL
1.	OVERTOPPING	30
2.	SEEPAGE	25
3.	SLIDES	15
4.	CONDUIT LEAKAGE	13
5.	SLOPE PAVING	5
6.	MISCELLANEOUS	7
7.	UNKNOWN	5
		100

FIG. 5.1 CAUSES OF INADEQUACIES OF EARTH DAMS
(BY T. A. MIDDLEBROOKS (1953))

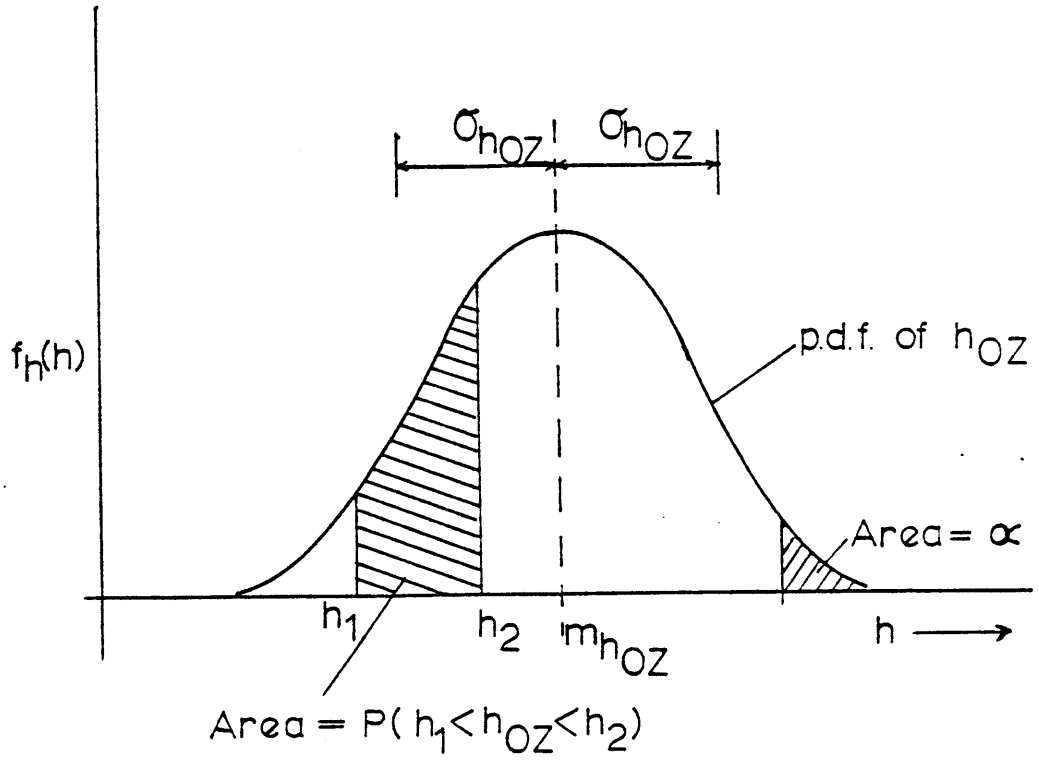

FIG. 5.2(a) PROBABILITY DENSITY FUNCTION (p.d.f) OF h_{OZ}

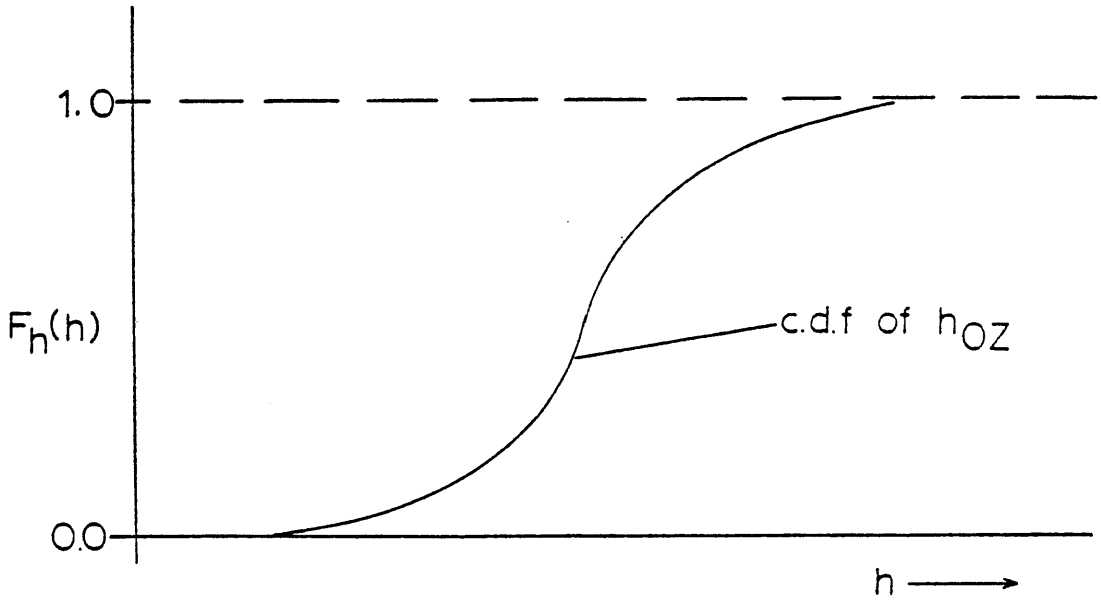

FIG. 5.2(b) CUMULATIVE DISTRIBUTION FUNCTION (c.d.f) OF h_{OZ}

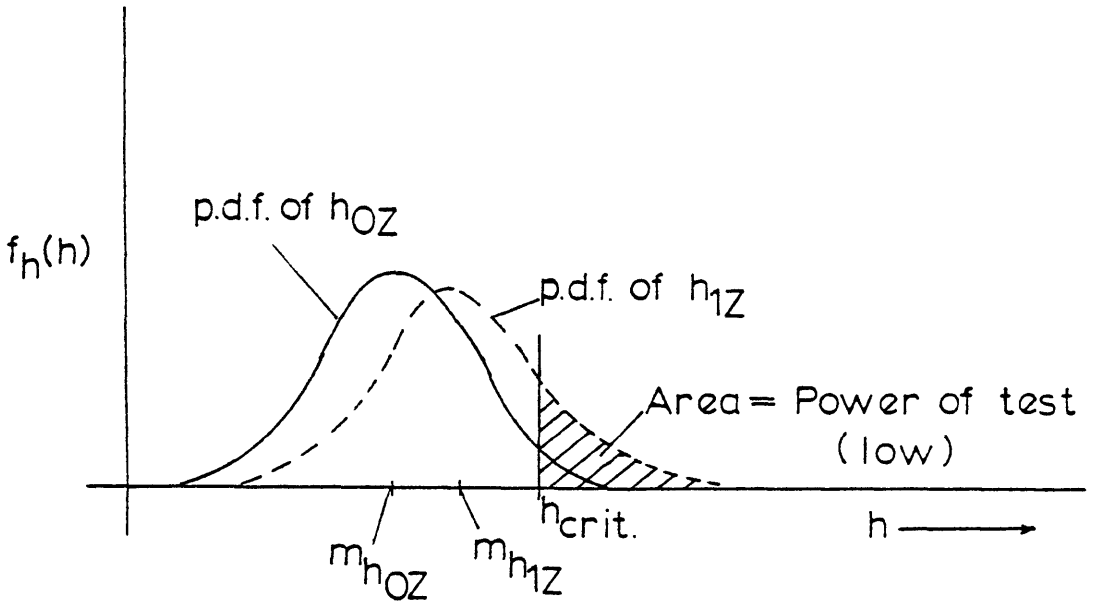

FIG. 5.3(a) POWER OF TEST WHEN $m_{h_{0Z}}$ AND $m_{h_{1Z}}$ ARE CLOSE TOGETHER

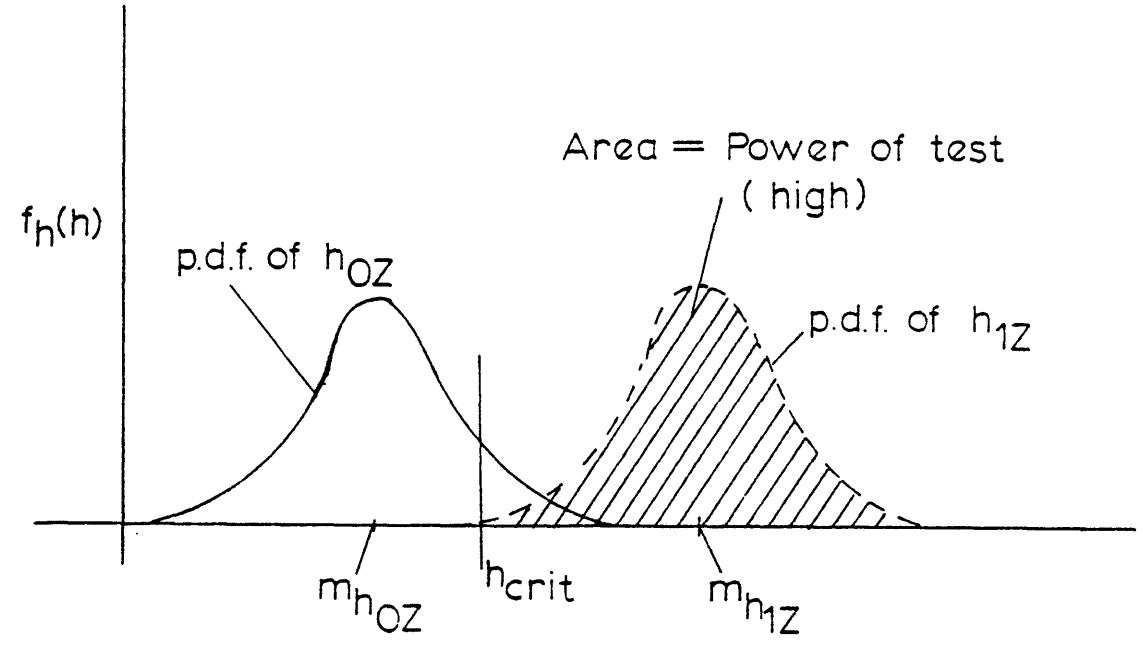

FIG. 5.3(b) POWER OF TEST WHEN $m_{h_{0Z}}$ AND $m_{h_{1Z}}$ ARE FAR APART

ACTUAL STATE OF NATURE / DECISION	H_0 IS TRUE	H_0 NOT TRUE
REJECT H_0	α TYPE 1 ERROR (LEVEL OF SIGNIFICANCE)	$1-\beta$ POWER OF TEST
NOT REJECTING H_0	$1-\alpha$	β TYPE 2 ERROR

FIG. 5.4 MEANINGS OF α AND β

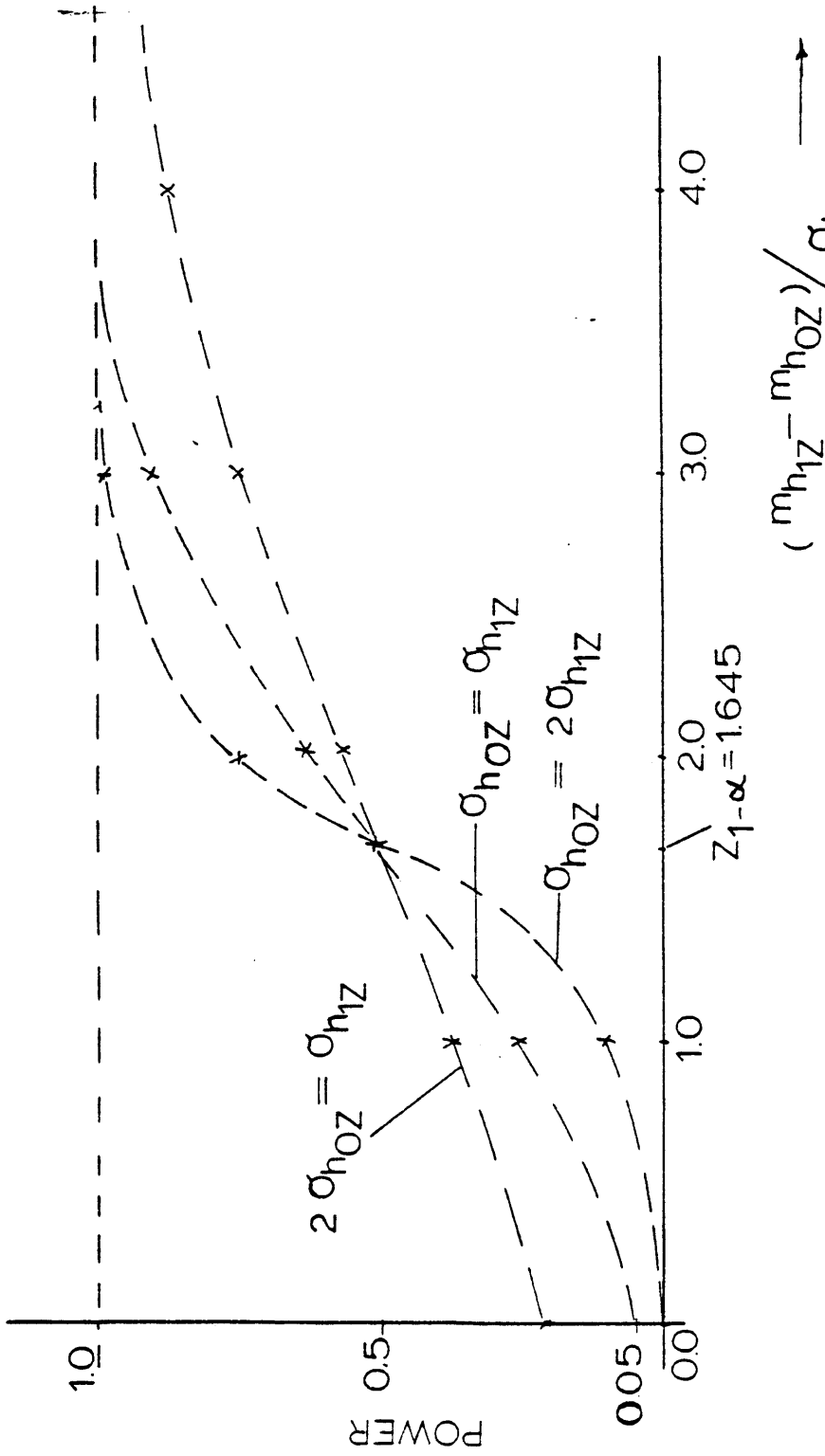

FIG. 5.5 POWER OF TEST AT DIFFERENT $\sigma_{h1Z}/\sigma_{h0Z}$, ($\alpha = 0.05$)

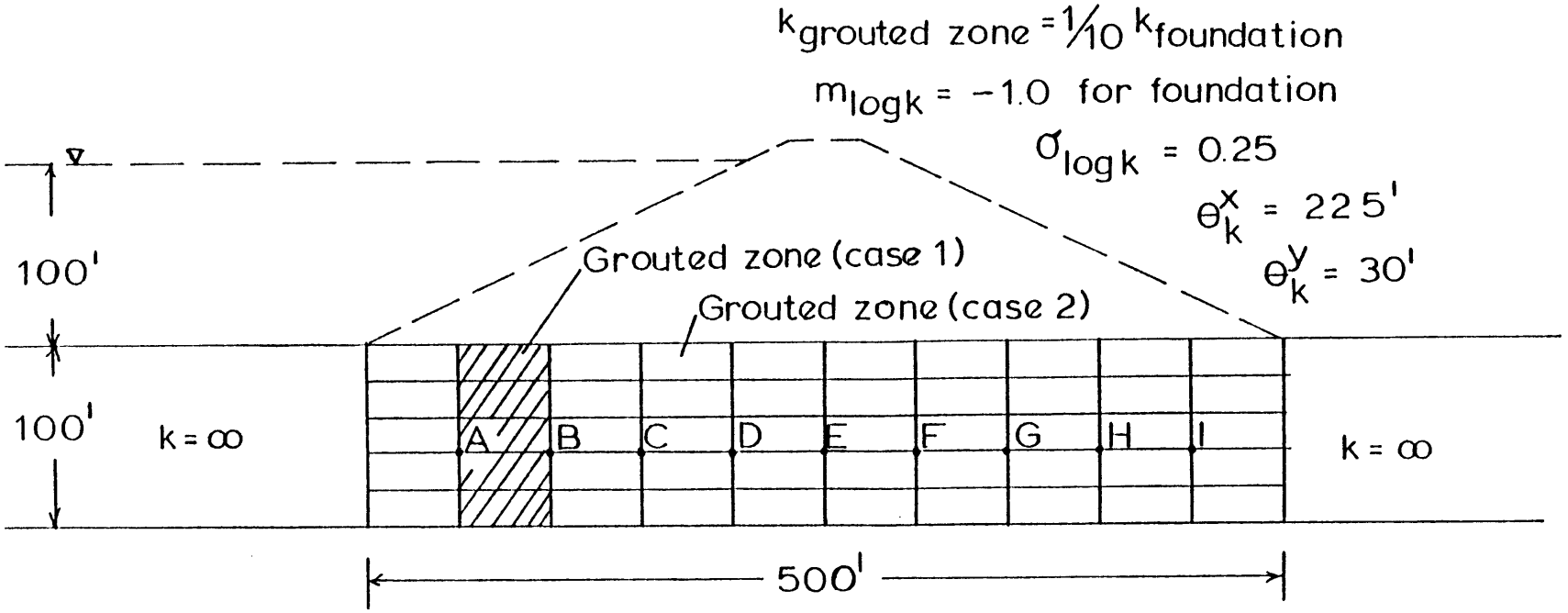

FIG. 5.6 GROUTING MODEL

NODES		A	B	C	D	E	F	G	H	I
H_0 (CASE 1)	$m_{h_{0Z}}$	94.7	42.1	36.8	31.6	26.3	21.1	15.6	10.5	5.3
	$\sigma_{h_{0Z}}$	1.04	7.60	7.78	7.55	6.94	5.97	4.73	3.34	1.78
H_1	$m_{h_{1Z}}$	90.0	80.0	70.0	60.0	50.0	40.0	30.0	20.0	10.0
	$\sigma_{h_{1Z}}$	2.75	4.85	6.36	7.30	7.63	7.30	6.36	4.85	2.75
POWER OF TEST, CASE 1		0.855	1.000	0.999	0.984	0.946	0.891	0.851	0.794	0.740
H_0 (CASE 2)	$m_{h_{0Z}}$	94.7	89.5	84.2	31.6	26.3	21.1	15.6	10.5	5.3
	$\sigma_{h_{0Z}}$	1.55	2.63	3.21	6.36	6.26	5.71	4.75	3.41	1.82
POWER OF TEST, CASE 2		0.785	0.855	0.919	0.992	0.961	0.904	0.848	0.788	0.739

TABLE 5.1 Summary of results from the grouting model

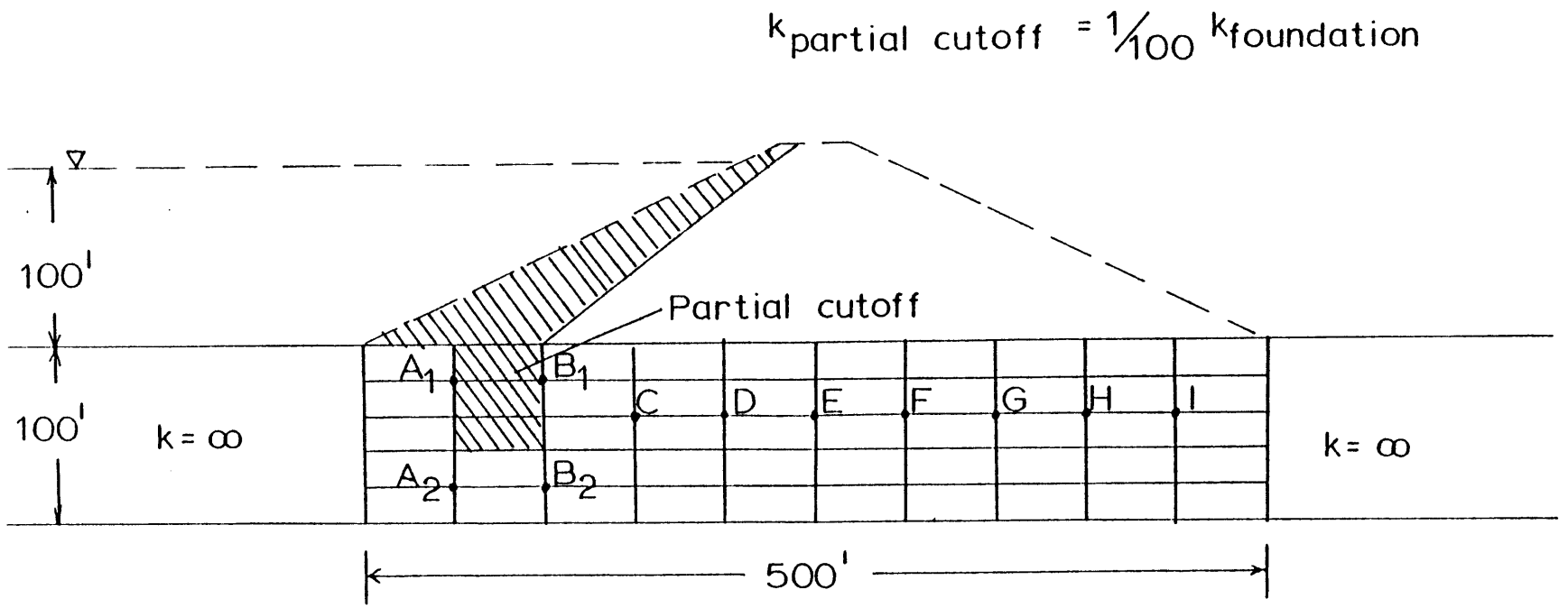

FIG. 5.7 PARTIAL CUTOFF MODEL

NODES		A1	A2	B1	B2	C	D	E	F	G	H	I
H_0	$m_{h_{0Z}}$	96.4	87.5	59.4	68.9	55.8	48.0	40.1	32.1	24.0	16.0	8.0
	$\sigma_{h_{0Z}}$	1.00	3.17	8.58	7.29	8.78	8.74	8.28	7.39	6.09	4.44	2.43
H_0	$m_{h_{1Z}}$	90.0	90.0	80.0	80.0	70.0	60.0	50.0	40.0	30.0	20.0	10.0
	$\sigma_{h_{1Z}}$	2.75	2.75	4.85	4.85	6.36	7.30	7.61	7.30	6.36	4.85	2.75
POWER OF TEST		0.958	0.163	0.910	0.427	0.486	0.373	0 313	0 281	0.264	0.248	0.235

TABLE 5.2 Summary of results from the partial cutoff model

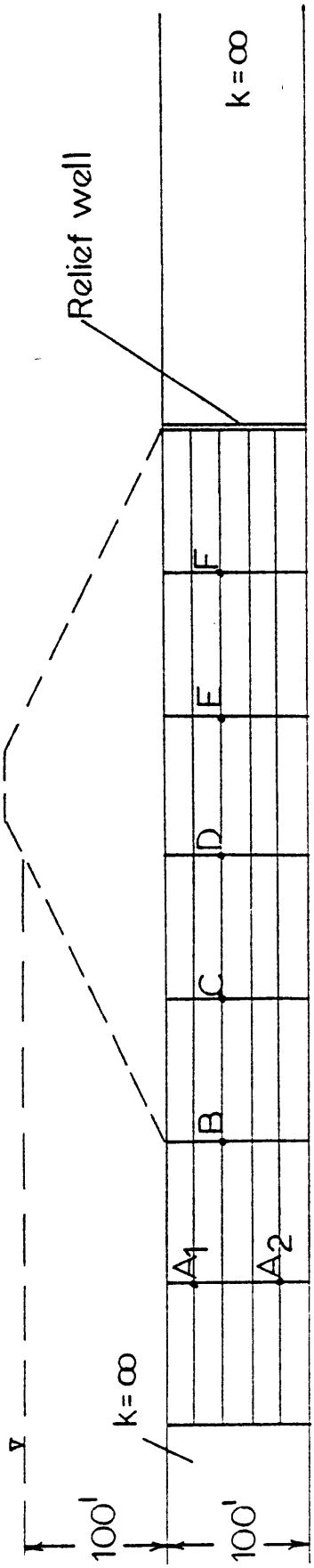

FIG. 5.8 RELIEF WELL MODEL

NODES		A1	A2	B	C	D	E	F
H_0	$m_{h_{0Z}}$	99.6	98.6	94.6	75.8	56.7	37.8	18.9
	$\sigma_{h_{0Z}}$	0.30	0.72	1.82	5.70	7.69	7.41	4.82
H_1	$m_{h_{1Z}}$	99.6	98.6	94.9	77.0	59.0	41.1	23.0
	$\sigma_{h_{1Z}}$	0.28	0.68	1.73	5.47	7.51	7.51	5.47
POWER OF TEST		0.050	0.050	0.061	0.068	0.084	0.119	0.242

TABLE 5.3 Summary of results from the relief well model

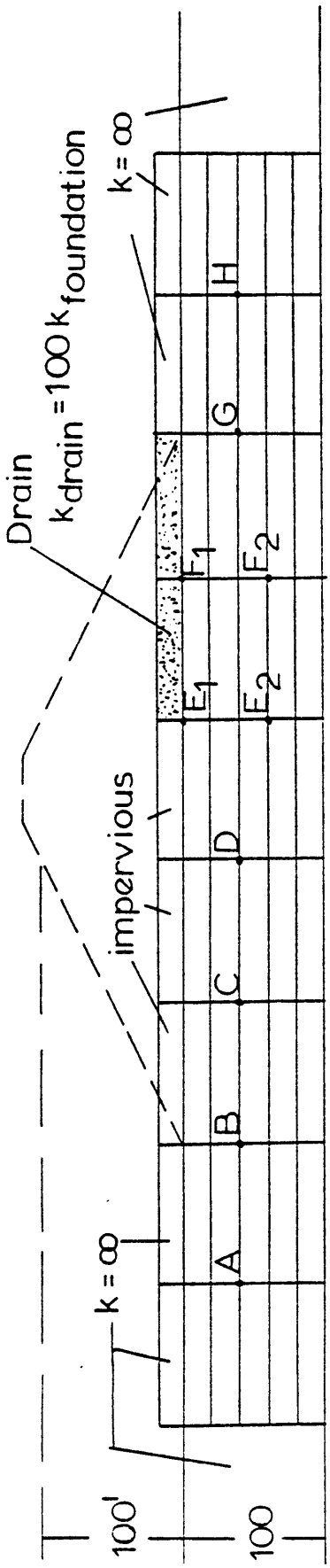

FIG. 5.9 DRAIN MODEL

NODES		A	B	C	D	E1	E2	F1	F2	G	H
H_0	$m_{h_{0Z}}$	98.8	92.1	64.9	37.1	2.31	11.9	1.27	3.02	0.53	0.10
	$\sigma_{h_{0Z}}$	0.73	2.53	6.89	6.96	0.87	3.12	0.52	1.17	0.28	0.07
H_1	$m_{h_{1Z}}$	99.2	94.9	77.0	59.0	41.0	41.0	23.5	23.0	5.20	0.80
	$\sigma_{h_{1Z}}$	0.48	1.73	5.47	7.51	7.51	7.49	5.59	5.43	1.74	0.51
POWER OF TEST		0.050	0.216	0.556	0.917	1.000	0.999	1.000	0.999	0.992	0.873

TABLE 5.4 Summary of results from the drain model

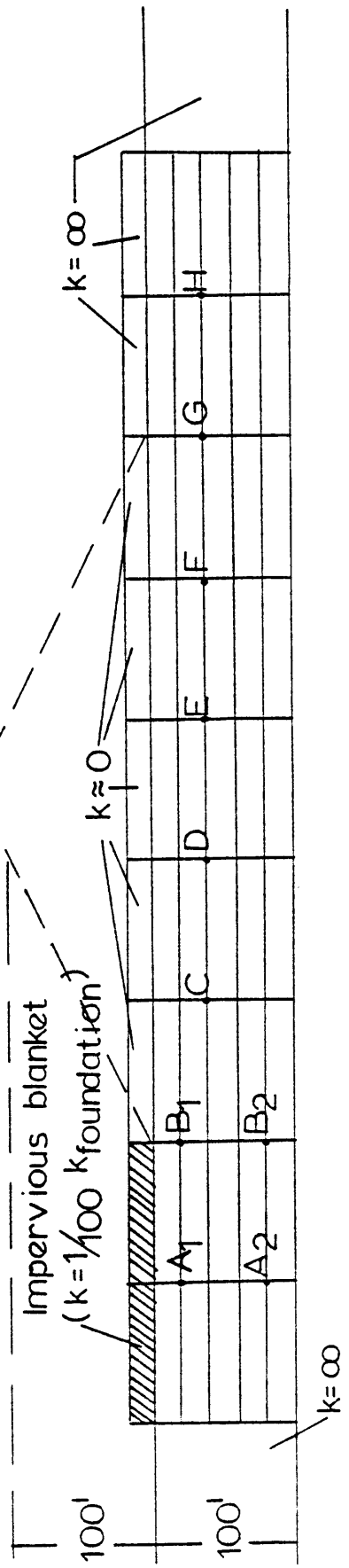

FIG. 5.10 IMPERVIOUS BLANKET MODEL

NODES		A1	A2	B1	B2	C	D	E	F	G	H
H_0	$m_{h_{0Z}}$	87.4	87.2	74.0	73.8	59.9	45.9	32.0	17.9	4.00	0.60
	$\sigma_{h_{0Z}}$	3.28	3.38	5.65	5.68	6.94	7.19	6.44	4.45	1.36	0.38
H_1	$m_{h_{1Z}}$	99.6	98.6	96.9	92.8	77.0	59.0	41.1	23.0	5.20	0.80
	$\sigma_{h_{1Z}}$	0.28	0.68	1.16	2.18	5.47	7.51	7.51	5.47	1.74	0.51
POWER OF TEST		1.000	1.000	1.000	1.000	0.849	0.568	0.421	0.343	0.278	0.202

TABLE 5.5 Summary of results from the impervious blanket model

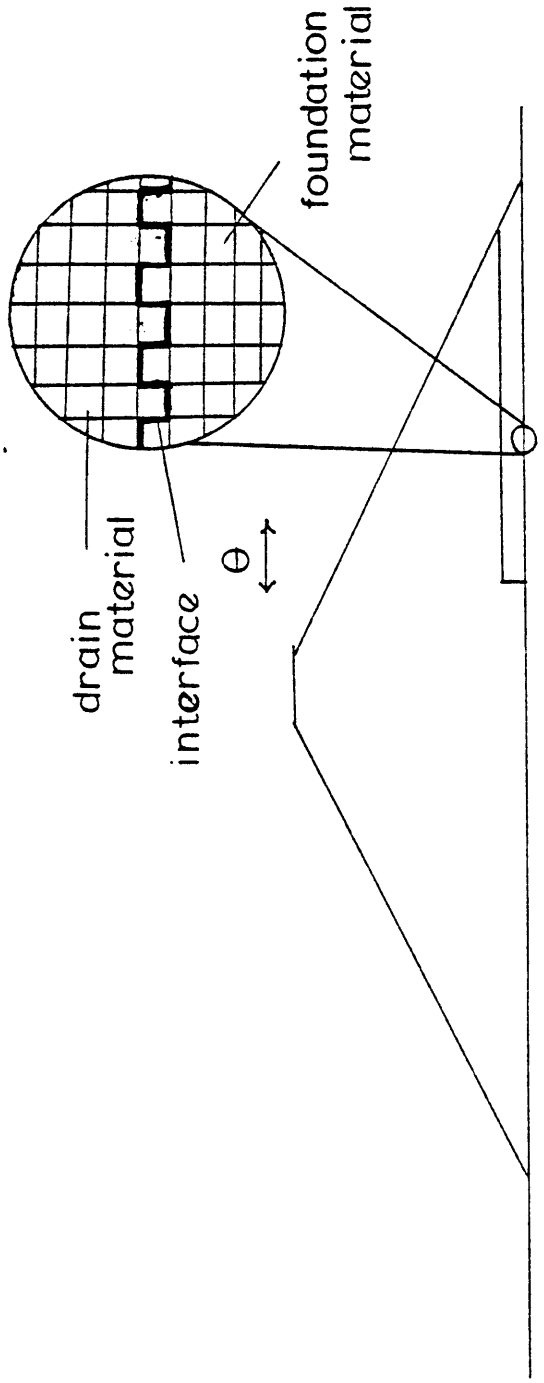

FIG. 5.11 MODEL TO STUDY PIPING AND INTERNAL EROSION

CHAPTER VI SUMMARY AND CONCLUSIONS

Chapter II of this thesis describes a simple and practical procedure based on a first-order second-moment approximation for evaluating the uncertainty of piezometric heads due to the inherent variability of permeability. The validity of the FOSM approach is proven when it was shown in Chapters II and III that the results from FOSM analysis of one- and two-dimensional underseepage models agree very well with the results obtained by other investigators (such as Freeze (1975), Dettinger (1979)). Through parametric studies of the one- and two-dimensional models, the following are found to govern the magnitude of the uncertainty of piezometric heads:

(i) the standard deviation of the permeability,

(ii) the vertical and horizontal scales of fluctuation of the permeability,

(iii) the sensitivity of piezometric heads to a change in permeability,

(iv) the presence of boundaries with known piezometric heads.

There are many practical applications of the proposed approach. In Chapter V, the FOSM analysis is applied to the study of active seepage control features in dam foundations. FOSM approach permits an engineer to predict σ_h at any location within a dam foundation under H_0 and H_1, the null and alternate hypotheses about the state of the dam. By using a statistical procedure called hypothesis testing described in Section 5.4, an engineer can derive useful information about the condition of a dam based on piezometer readings.

The current approach, besides yielding reliable estimates of the

uncertainty of piezometric measurements, also has the following advantages:

(i) It is a computationally efficient method of studying seepage uncertainty. The outcome of the analysis is not sensitive to the degree of discretization, and therefore only a minimal degree of discretization is needed to ensure the convergence of the results (see Section 3.2(a)).

(ii) Although linearization is involved in the basic methodology, proper correction for nonlinearity is possible following the equivalent slope method in Section 3.2(e).

(iii) The approach is versatile. Because there are not many assumptions in the approach, it can be applied to the study of a wide range of practical problems discussed in Chapter V.

(iv) The approach also yields useful information about the spatial correlation of piezometric heads which can facilitate interpretation of adjacent piezometer readings.

There are few restrictions to the general applicability of the current approach. An important restriction is that it only deals with seepage uncertainty under steady state seepage condition. In this study, useful information about the sensitivity of the variability and correlation of piezometric head is generated based on assumed statistical parameters of the permeability. So, another restriction is that application of the approach is only possible if reliable estimates of the statistical parameters of permeability can be obtained.

REFERENCES

Bakr, A. A., "Stochastic Analysis of the Effect of Spatial Variations in Hydraulic Conductivity on Groundwater Flow," Ph.D. Dissertation, N. Mex. Inst. of Mining and Technol., Socorro, July (1976).

Bakr, A. A., L. W. Gelhar, A. L. Gutjahr, J. R. MacMillan, "Stochastic Analysis of Spatial Variability in Subsurface Flows, 1, Comparison of One- and Three-Dimensional Flows," Water Resources Research, 14(2), 263-71, (1978).

Bear, J., Dynamics of Fluids in Porous Media, 764 pp., Elsevier, (1972).

Benjamin, J. R., Cornell, C. A., Probability, Statistics, and Decisions for Civil Engineers, McGraw Hill, (1970).

Bertram, G. E., "An Experimental Investigation of Protective Filters," Publication of the Graduate School of Engineering, Harvard University, No. 267, January, (1940).

Cedergren, H. R., "Seepage Requirements of Filters and Pervious Bases," Proc. ASCE 86, SM5, 15, (1960).

Dagan, G., "Models of Groundwater Flow in Statistically Homogeneous Porous Formations," Water Resour. Res., 15(1), 47-63, (1979).

DeMello, V. F. B., "Reflections on Design Decisions of Practical Significance to Embankment Dams," Geotechnique 27, No. 3, 279-335, (1970).

Dettinger, M. D., "Numerical Modelling of Aquifer Systems Under Uncertainty: A Second Moment Analysis," MIT Dept. of Civil Engr., M.S. Thesis, May (1979).

Freeze, R. A., "A Stochastic-Conceptual Analysis of One-Dimensional Ground-Water Flow in Nonuniform Nonhomogeneous Media," Water Resour. Res., 11(5), 725-41, (1975).

Hachich, W., "Seepage Related Reliability of Embankment Dams," MIT Dept. of Civil Engr., Ph.D. Thesis, Aug. (1980).

ICOLD (International Committee on Large Dams) Committee on Failures and Accidents to Large Dams, "Lessons from Dam Incidents," (1974).

Karpoff, K. P., "The Use of Laboratory Tests to Develop Design Criteria for Protective Filters," Proc. ASTM, Vol. 55, p. 1183, (1955).

Kassif, G., Zaslavsky, D., Zeitlen, J. T., "Analysis of Filter Requirements for Compacted Clays," Proc. 6th Int. Conf. of Soil Mech. and Fdn. Engr., Montreal 2, 495-99, (1965).

Marr, W. A., Lambe, T. W., "Predicted and Measured Pore Pressures in a Dam," Proc. of the Specialty Conf. on Computers in Soil Mech., Present and Future, 9th Int. Conf. on Soil Mech. and Fdn. Engr., Tokyo, p. 124-142, July (1977).

Matthews, G., "Predicted and Measured Pore Pressures in Dams," MIT Dept. of Civil Engr. M.S. Thesis, (1980).

Middlebrooks, T. A., "Earth Dam Practice in the United States," ASCE Transaction, Vol. CT, 697-722, (1953).

Moseley, S., "Stochastic Analysis of Seepage," MIT Dept. of Civil Engr., M.S. Thesis, (1978).

Peck, R. B., "Advantages and Limitations of Observational Method in Applied Soil Mechanics," Geotechnique 19, No. 2, 171-187, (1969).

Sagar, B., "Galerkin Finite Element Procedure for Analysing Flow Through Random Media," Water Resour. Res., 14(6), 1035-44, (1978).

Schmidheini, T. A., "Transient Flow Analysis in Dam Safety," MIT Dept. of Civil Engr., M.S. Thesis, (1978).

Sherard, J. L., et. al., "Piping in Earth Dams of Dispersive Clay," Performance of Earth and Earth-Supported Structures, Part 1, ASCE, 589, (1972).

Silveria, A., "An Analysis of the Problem of Washing Through in Protectice Filters," Proc. 6th Int. Conf. of Soil Mech. and Fdn. Engr., Montreal, 2, 551, (1965).

Smith, L., Freeze, R. A., "Stochastic Analysis of Steady State Groundwater Flow in a Bounded Domain, 1., One-Dimensional Simulations," Water Resour. Res., 15(3), 521-28, (1979).

Taylor, R. L, Brown, C. B., "D'arcy Flow Situation with a Free Surface," ASCE, 93, HY2, 25-33, (1967).

Terzaghi, K., "Der Grundbrunch au Stauwerken und Seine Verhutung," Forcheimer-Nummer Wasserkr. 17, p. 445-449, (1922).

U.S. Army Corps of Engineers Waterway Experimental Station, "Investigation of Filter Requirements for Underdrains," Technical Memorandum, No. 183-1, December (1941).

Vanmarcke, E. H., "On the Scale of Fluctuation of Random Functions," MIT Dept. of Civil Engr. Research Report, R79-19, (1979a).

Vanmarcke, E. H., "Averages and Extremes of Random Fields," MIT Dept. of Civil Engr. Research Report, R79-43, (1979b).

Warren, J. E., Price, H. S., "Flow in Heterogeneous Porous Media," Soc. Petrol. Eng. J., 1, 153-169, (1961).

Willardson, L. S., Hurst, R. L., "Sample Size Estimates in Permeability Studies," ASCE, 91, IR 1, 1-9, (1965).

APPENDIX

Fig. A1 shows a general 1-D underseepage model where:

number of elements = m

number of nodes = $m + 1$

head drop in element i = ΔH_i

permeability of element i = k_i

upstream head = h_0

downstream head = h_m

Since the flow through all the elements is constant, we have:

$$k_1 \Delta H_1 = k_2 \Delta H_2 = \ldots = k_m \Delta H_m$$

$$\Delta H_a = \frac{k_b \Delta H_b}{k_a} \tag{A1}$$

a and b are any arbitrary constants.

Sum of all head drops = $h_0 - h_m$.

Therefore:

$$\sum_{a=1}^{m} \Delta H_a = h_0 - h_m = \sum_{a=1}^{m} \Delta H_b \frac{k_b}{k_a}$$

$$\Delta H_b = \frac{h_0 - h_m}{\sum_{a=1}^{m} \frac{k_b}{k_a}} \tag{A2}$$

At node j:

$$h_j = h_0 - \sum_{b=1}^{j} H_b$$

$$= h_0 - \sum_{b=1}^{j} \frac{h_0 - h_m}{\sum_{a=1}^{m} \frac{k_b}{k_a}}$$

Therefore:

$$h_j = h_0 - \frac{h_0 - h_m}{(\frac{1}{k_1}+\frac{1}{k_2}+\ldots+\frac{1}{k_m})} (\frac{1}{k_1}+\frac{1}{k_2}+\ldots+\frac{1}{k_j}) \qquad \text{(A3)}$$

which is identical to Eq. 3.1

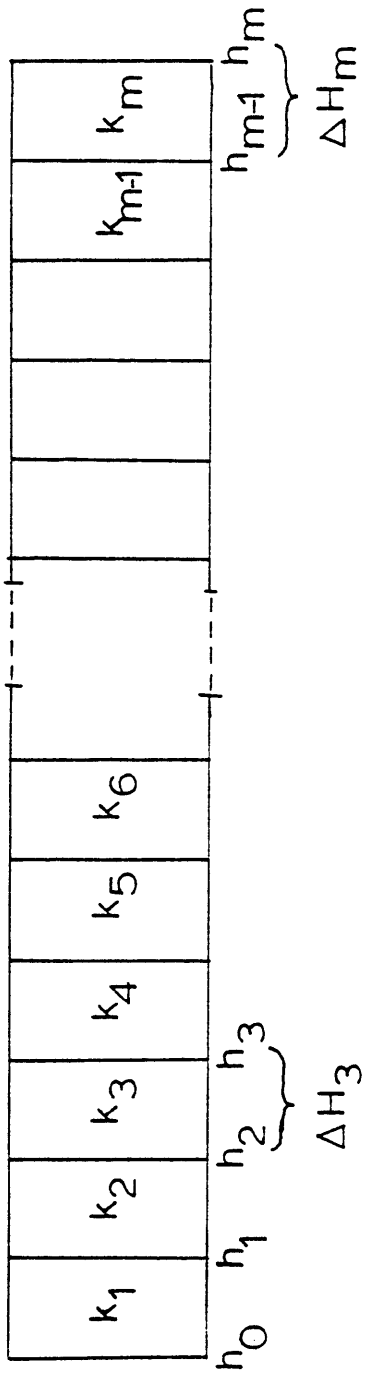

FIG. A1 A GENERAL 1-D UNDERSEEPAGE MODEL